

Hierarchically Structured Bioinspired Nanocomposites

Dhriti Nepal,¹ Saewon Kang,² Katarina M. Adstedt,³ Krishan Kanhaiya,⁴ Michael Rainer Bockstaller,⁵ L. Catherine Brinson,⁶ Markus J. Buehler,⁷ Peter V. Coveney,⁸ Kaushik Dayal,⁹ Jaafar A. El-Awady,¹⁰ Luke Christian Henderson,¹¹ David L. Kaplan,¹² Sinan Keten,¹³ Nicholas A. Kotov,¹⁴ George C. Schatz,¹⁵ Silvia Vignolini,¹⁶ Fritz Vollrath,¹⁷ Yusu Wang,¹⁸ Boris I. Yakobson,^{19,20} Vladimir V. Tsukruk,²¹ Hendrik Heinz²²

¹ Materials and Manufacturing Directorate, Air Force Research Laboratory, Wright-Patterson AFB, Dayton, Ohio 45433

² School of Materials Science and Engineering, Georgia Institute of Technology, Atlanta, GA 30332

³ School of Materials Science and Engineering, Georgia Institute of Technology, Atlanta, GA 30332

⁴ Department of Chemical and Biological Engineering, University of Colorado at Boulder, Boulder, CO 80301

⁵ Department of Materials Science and Engineering, Carnegie Mellon University, Pittsburgh, PA 15213

⁶ Department of Mechanical Engineering and Materials Science, Duke University, Durham, NC 27708

⁷ Department of Civil and Environmental Engineering, MIT, Cambridge, MA 02139

⁸ Department of Chemistry, University College London, London, WC1E 6BT, UK

⁹ Department of Civil and Environmental Engineering, Carnegie Mellon University, Pittsburgh, PA 15213

¹⁰ Department of Mechanical Engineering, Johns Hopkins University, Baltimore, MD 21218

¹¹ Institute for Frontier Materials, Deakin University, Waurn Ponds VIC 3216, Australia

¹² Department of Biomedical Engineering, Tufts University, Medford, MA 02155

¹³ Department of Mechanical Engineering, Northwestern University, Evanston, IL 60208

¹⁴ Department of Chemical Engineering, University of Michigan, Ann Arbor, MI 48109

¹⁵ Department of Chemistry, Northwestern University, Evanston, IL 60208

¹⁶ Department of Chemistry, University of Cambridge, Cambridge CB2 1EW, UK

¹⁷ Department of Zoology, University of Oxford, Oxford OX2 8QJ, UK

¹⁸ Halicioğlu Data Science Institute, University of California San Diego, La Jolla, CA 92093

¹⁹ Department of Materials Science and Nanoengineering, Rice University, Houston, TX 77005

²⁰ Department of Chemistry, Rice University, Houston, TX 77005

²¹ School of Materials Science and Engineering, Georgia Institute of Technology, Atlanta, GA 30332

²² Department of Chemical and Biological Engineering, University of Colorado at Boulder, Boulder, CO 80301

Corresponding authors: Dhriti Nepal, dhriti.nepal.1@afrl.af.mil; Vladimir Tsukruk, vladimir@mse.gatech.edu; Hendrik Heinz, hendrik.heinz@colorado.edu

37

38 **Abstract**

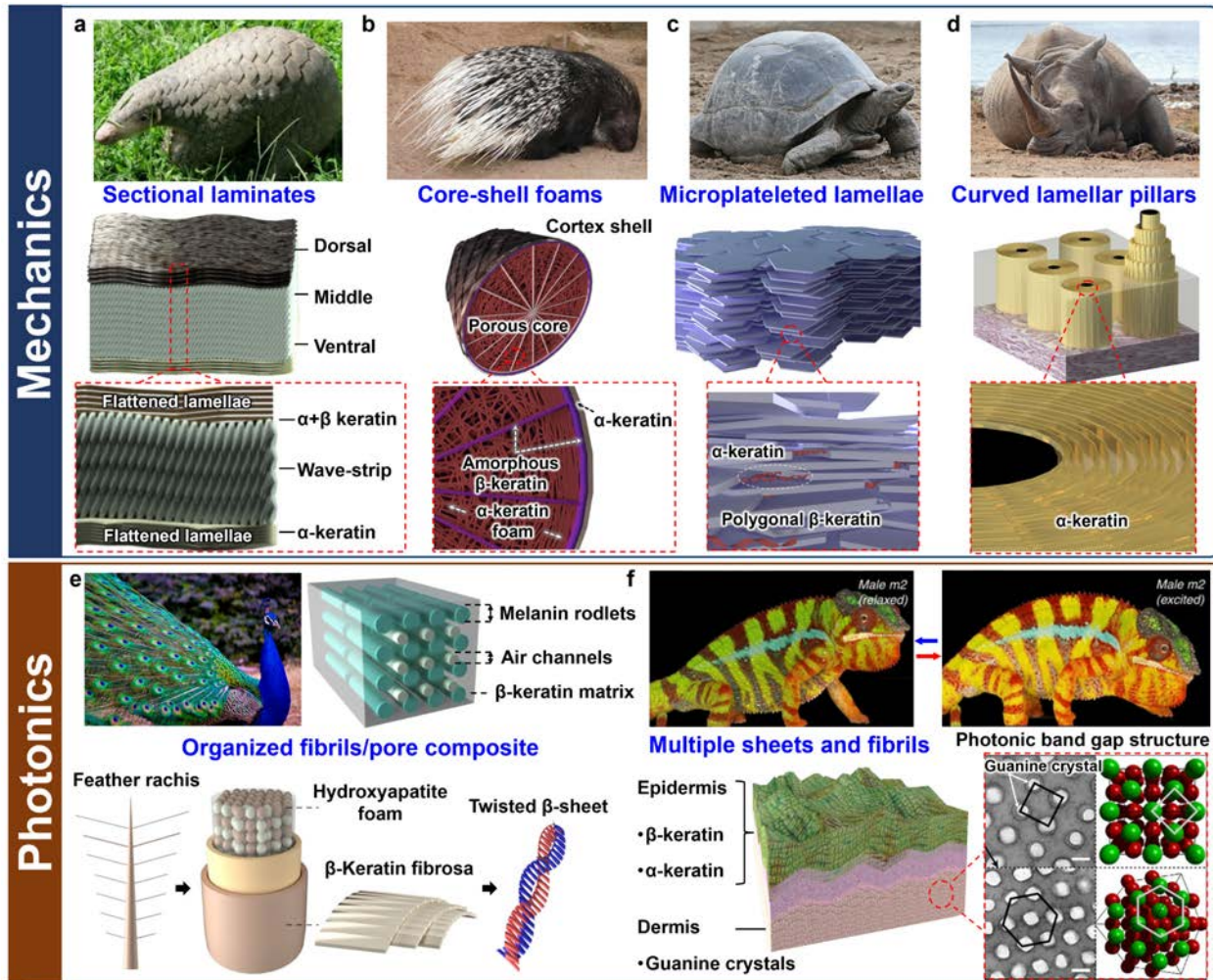
39 Next-generation structural materials are expected to be lightweight, high strength, and tough
40 composites with embedded functionalities to sense, adapt, self-repair, morph, and restore. This
41 review highlights recent developments and concepts in bioinspired nanocomposites, emphasizing
42 tailoring the architecture, interphases, and confinement to achieve dynamic and synergetic
43 responses. We highlight cornerstone examples from natural materials with unique mechanical
44 property combinations based on relatively simple building blocks produced in aqueous
45 environments at ambient conditions. A particular focus is on structural hierarchies across multiple
46 length scales to achieve multifunctionality and robustness. We further discuss recent advances,
47 trends, and emerging opportunities in combining biological and synthetic components, state-of-
48 the-art characterization, and modelling approaches to assess the physical principles underlying
49 nature design and mechanical responses at multiple length scales. These multidisciplinary
50 approaches promote the synergetic enhancement of individual materials properties and an
51 improved predictive and prescriptive design of the next era of structural materials at multi-length
52 scales for a wide range of applications.

53 1. Introduction

54 Nature has mastered the fabrication of hierarchical multifunctional materials, which in many ways
55 surpass their synthetic counterparts, in an evolutionary process over millions of years.^{1,2} The
56 astonishing results have been achieved by taking advantage of diverse fundamental molecular
57 interactions in a small set of building blocks at ambient conditions (Box 1). In particular, the
58 evolutionary development of multi-layer hierarchical structures with unique and sometimes
59 contradictory properties, such as combined high strength and toughness, provides great inspiration
60 for modern materials engineering. Mimicking nature's hierarchical microstructures in synthetic
61 composites can lead to more damage-tolerant architectures, and some bioinspired materials are
62 already implemented in various applications.³ The new frontiers lie in introducing sustainable,
63 hierarchical, and dynamic composites that are multifunctional and environmentally friendly.
64 Hereby, engineering of bioinspired structures faces many challenges, including the realization of
65 molecular-scale precision within each level of the hierarchy, structural coupling between hard and
66 soft building blocks, the retention of mechanical integrity while having a good balance of other
67 functional properties, as well as the ability for fast and large-scale production.

68 One grand challenge to developing bio-inspired composites is control over composition, gradients,
69 interfaces, microstructures, morphology, and responses under dynamic conditions. In certain
70 instances, synthetic composites are superior, for example, in the automotive and aerospace field
71 where temperature resistance is critical. Yet, bioinspired composites can be produced under eco-
72 friendly conditions by incorporating traditional design strategies and advanced synthetic materials,
73 resulting in exceptional properties. Studies on some of the most robust natural materials provide
74 insights into basic principles, especially the critical role of molecular interactions and hierarchical
75 architectures (Box 1a-f).^{2,4} The structural hierarchy enables multiple deformation, self-healing,
76 plasticity, and toughening mechanisms within the composites across length scales.⁵ For example,
77 at the nanometer scale (nm), architectures of compositional gradients and fuzzy interphases (3D
78 interfacial regions), as discovered in layer-by-layer assembled structures, facilitate intrinsic
79 toughening by chain slippage, stress delocalization, and non-destructive locking across organic
80 interfaces. Simultaneously at larger scales of micrometers (μm), hierarchical structures play a
81 pivotal role for extrinsic toughening such as crack-bridging and pull-out to dissipate energy via
82 weak or soft interfaces (see fundamental relationships in Box 1g, h).^{1,4} To harness such functions,
83 many organisms have developed an unparalleled ability to shape mineral-rich materials into
84 anisotropic structures to serve as load-bearing elements, which extend over several orders of
85 magnitude in size.⁶ The resulting combination of stiffness, strength, and toughness has fueled
86 research for synthetic bioinspired analogs because existing synthetic composite materials often
87 show increased strength at the expense of toughness or vice versa.

88 A second grand challenge in the modern materials world, which draws inspiration from nature, is
89 that scale-up synthesis and processing yet have to be mastered in industrial settings, including the
90 demand for added functionality on structural components.⁷ Multi-functional hierarchical materials
91 found in plants and living organisms include celluloses, keratins, and silk (Fig. 1, Box 1e, f). These
92 complex systems in nature are produced at a massive scale and engineered using relatively simple
93 building blocks and constituents under highly sustainable conditions, including aqueous
94 environments and ambient temperature.



95

96 Figure 1 | **Keratin-based hierarchical structures in different animal species.** A common feature of
 97 keratin-based hierarchical composites are precisely folded tertiary keratin structures, which control
 98 mechanics by means of layers, interfaces, and gradients, as well as co-assembly with other functional
 99 polymers or minerals to generate periodic order. **a** | Pangolin scales consist of α -keratin and β -keratin and
 100 are known for their distinctive protection mechanism. The scales comprise of an internal layered structure
 101 with densely packed keratinized flattened lamellae that are wavy and parallel to the external surface in
 102 dorsal and ventral regions, and elongated cellular morphology that are tilted and deformed in the middle
 103 region.⁸ **b** | Porcupine quills are composed of a keratin configuration that includes a stiff outer sheath and
 104 compliant porous core structures.⁸ **c** | Turtle shells are biomineralized structures constructed with
 105 compacted, ordered, and stacked polygonal keratin micro lamellae that have a high amount of β -keratin and
 106 a small quantity of α -keratin and minerals (calcium phosphate and calcium sulfate).⁹ **d** | Rhinoceros horns
 107 are made of α -keratin with a lamellar structure (2–5 μm in thickness) stacked in the radial direction with
 108 tubules (40–100 μm in diameter) dispersed between the lamellae, extending along the length of the horn in
 109 the growth direction.¹⁰ **e** | Peacock tail feathers are composed of parallel melanin rod bundles connected in
 110 a β -keratin matrix for 2D photonic structures, which generate magnificent iridescent colors. The feather's
 111 rachis contains branches of multi-colored barbs that derive their unique iridescence from parallelly oriented
 112 bundles of fibrils composed of two twisted β -sheets that consist of mostly hydroxyapatite foam and a small
 113 portion of cortex from β -keratin fibers.⁸ **f** | The panther chameleon shows a beautiful green striped color
 114 pattern due to guanine photonic crystals in the relaxed state. These colors change to a bright yellow in the

115 stressed state. The epidermis consists of highly keratinized layers of α -keratin and β -keratin, which give a
116 rough texture on the skin, defend against predators, and protect the softer and more adaptive photonic
117 crystals underneath the epidermis (scale bars are 200 nm).¹¹

118
119 We specifically highlight keratin, a critical component of many natural structures, as an
120 inspirational source (Fig. 1).⁸ Keratin is a structural protein in hair, horn, and hoof (Box 1f) that
121 serves as a robust yet soft material in the exoskeleton of a wide range of vertebrates (Fig. 1). The
122 exoskeleton of animals exhibits multiple functions: self-defense, communication, sensing, and
123 temperature regulation, albeit each process uses different mechanisms facilitated by complex
124 hierarchical structures and composition gradients. We categorize examples of these keratin-based
125 multi-functional hierarchical structures from six distinct animal species based on their two primary
126 functions: mechanics and photonics (Fig. 1). One major function of horn and hoof is impact
127 resistance and energy absorption.¹² More subtly, keratin functions as defensive shielding in the
128 skin via a complex curved architecture in pangolin scales (Fig. 1a),⁸ a piercing weapon in
129 porcupine quills (Fig. 1b),⁸ sturdy protection via ordered stacks in turtle shells (Fig. 1c),⁹ and in
130 rhinoceros horn (Fig. 1d).¹⁰ These hierarchical structures vary in their shape from waved stripes of
131 cellular morphology in multilayered laminates (Fig. 1a) to amorphous foams (Fig. 1b), to
132 microplatelet-containing lamellae of turtle shells (Fig. 1c) and curved lamellar pillars in rhinoceros
133 horns (Fig. 1d). All these hierarchical structures achieve the function of dissipating energy for self-
134 defense. In one specific structure, the pangolin scale's multilayered laminates, the lamellar
135 structures exhibit unusual crack deflection with non-uniform crack profiles (Fig. 1a). Interlamellar
136 shearing of the keratin interfaces leads to tablet sliding and inelastic regions surrounding cracks,
137 resulting in enhanced fracture toughening.¹³ The microtubule structures serve as a stiff
138 reinforcement that supports the entire wall and prevents catastrophic failure under impact loading
139 via inherently viscoelastic properties of keratin.¹² These hierarchical layered architectures are
140 necessary for penetration-resistance and dissipating energy within the sub-layers, helping to
141 delocalize stresses and damages while being environmentally resilient under extreme fluctuations
142 in humidity and temperature.

143 In contrast to direct structural applications related to self-defense, keratin can be combined with
144 periodic inclusions of melanin rods to form photonic crystals with the bright, vivid coloration
145 found in many bird's feathers, including peacock feathers (Fig. 1e). Keratin can also provide
146 structural protection of guanine nanocrystals for color adaptivity in the chameleon dermis (Fig.
147 1f).¹¹ Both of these photonic structures employ fibrillar architectures, as seen by organized fibrils
148 and pores in peacocks' feather frames (Fig. 1e), as well as multiple sheets and fibrils in chameleon
149 skin (Fig. 1f). These complex keratin-based hierarchical structures illustrate examples of
150 multifunctionality, while being mechanically resilient,^{12,13} fulfilling essential roles for defense,
151 stress signaling, courtship display through structural color, and thermal protection.¹¹

152 Elucidating the underlying mechanisms and correlated functions of such complex structures still
153 poses a tremendous challenge for the scientific community. Understanding the design principles
154 provides opportunities to incorporate various functions in synthetic systems such as photonics and
155 morphing while enhancing mechanical integrity. The goal of 'emulating nature's design
156 principles' can also be accelerated through interactive, real-time feedback in synthesis and
157 characterization by utilizing opportunities in machine learning (ML), data science, artificial
158 intelligence (AI), and additive manufacturing (AM).

159 Based on structure-function prototypes found in nature and recent studies, this review examines
160 recent breakthroughs, trends, and advances in the design, synthesis, and understanding, of nature-
161 inspired hierarchical bioinspired materials. We emphasize on how weak and strong chemical
162 interactions can be configured to create synthetic hierarchical architectures with tight control over
163 morphology, structure, function, appearance, and mechanics at different length scales, across time
164 scales, and force scales. We identify critical challenges for designing future structural materials
165 with added functionalities and discuss how an interdisciplinary era of materiomics, that harnesses
166 big data, could accelerate the development of the next generation of advanced materials by linking
167 material structure to properties and functions.

168

169 **2. Hierarchy of interactions and energy across scales**

170 The unique combination of mechanical and functional properties in natural materials is associated
171 with the hierarchical organization at various length scales, that can also change with time, from
172 molecular ordering to macroscale assembly (Fig. 2, Hierarchical structures). Such synergetic self-
173 organization is mediated by ubiquitous, highly structured, hard-soft interfaces.¹⁴ A common
174 feature of these interfaces is ‘deliberate imperfection,’ i.e., a designed degree of complexity not
175 found in engineered materials.

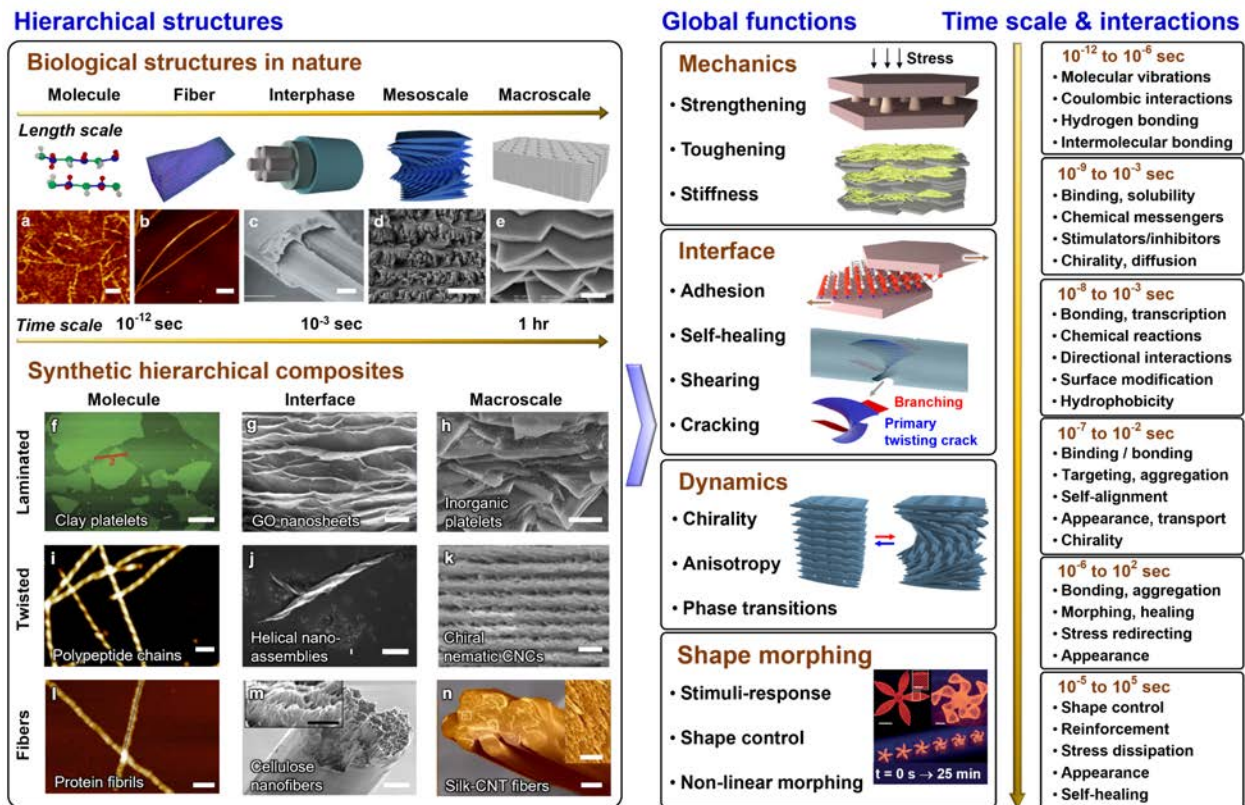
176 The spatial dimensions of hierarchical structures vary greatly depending on end-goal functionality
177 and volume constrains from 0 dimensions (0D) to N dimensions (ND). ND may also incorporate
178 further dimensions such as time or other responsive changes in the material. The dimensions of
179 these ND structures further influence the size and subsequent interactions of the molecules and
180 interfaces and the eventual, multi-level, macro-scale material structure, such as twisted, laminated,
181 or fibrous composites (Fig. 2, Hierarchical Structures). Hierarchical structures can span beyond
182 singular dimensions, evidenced by the organization of peptides into nanoscale sheets and their
183 subsequent organization into fibrillar structures that bundle to form large-scale fibrillary and
184 laminated solids (Fig. 2, Hierarchical structures, a-e). The assembly into laminated and fibrillar
185 structures defines a higher level of organization of interfaces and nanostructures in large-scale
186 bioinspired and synthetic inorganic-organic materials (Fig. 2, Hierarchical structures, f-n).

187 Ultimately, the combination of strong and weak interfaces determines the toughness, strength, and
188 stiffness of a material, along with its shear and adhesive properties (Fig. 2, Global functions, two
189 top panels). A prominent example from nature that employs strong and weak interfaces for energy
190 dissipation is nacre, which features a “brick-and-mortar” configuration with relatively stiff
191 aragonite bricks and soft biological material as the mortar. A small fraction (~5%) of protein binder
192 is sufficient to significantly increase fracture toughness as it allows the aragonite bricks to slide,
193 dissipating energy while retaining the overall high stiffness.¹⁵ Reversible reorganization of
194 interfaces, driven by induced phase and molecular transformations, facilitates a dynamic behavior
195 that allows nature to modulate shape and stimuli-responsive properties (Fig. 2, Global functions,
196 two bottom panels). Morphing and responsive behavior are realized by a variety of molecular
197 mechanisms, such as re-alignment or re-bonding of functional groups, molecules, and
198 nanoparticles. The processes of bonding, reactions, relaxation, and diffusion of structural elements
199 range from picoseconds to millisecond timescales (Fig. 2, Time scale and interactions).
200 Furthermore, materials-forming processes include aggregation, crystallization, dissolution, phase

201 separation, relaxation, controlled deformation, appearance, morphing, and self-healing of
 202 hierarchical materials across similar time scales.

203 Therefore, it is challenging to develop synthetic hierarchical structures with the mechanical
 204 resilience (Box 1g) and functionalities that nature can offer.¹⁶ It remains difficult to re-create and
 205 program the complexity of diverse components and interfaces, which combine different phases,
 206 create material gradients, and enable reversible energy dissipation, with incredible control over
 207 local and global mechanics, into synthetic processes. We will examine the processes through which
 208 materials acquire multiple functionalities in the next section.

209



210
 211 **Figure 2 | Hierarchical bio-inspired composite designs in terms of spatial and time scales and major**
 212 **contributions in mechanical functionality.** Representative hierarchical biological structures from nature,
 213 schematics (top panels) and actual morphologies including, **a** | AFM topographical image of β -sheet
 214 secondary structure of silk fibroin (scale bar is 50 nm),¹⁷ **b** | AFM topography of silk nanofibrils (scale bar
 215 is 0.5 μm),¹⁸ **c** | SEM image of single-filament silkworm silk fibers (scale bar is 5 μm),¹⁹ **d** | SEM image of
 216 hierarchical Bouligand structure of the dactyl club of the stomatopod (scale bar is 20 μm),²⁰ **e** | SEM cross-
 217 section image of natural *Cristaria plicata* nacre with hierarchical layered microstructure (scale bar is 1 μm).²¹
 218 Synthetic and hybrid composite materials morphologies include **f** | AFM image of polyvinylalcohol (PVA)
 219 coated core-shell clay nanoplatelets (scale bar is 1 μm),²² **g** | SEM image of layered nanostructure of
 220 graphene oxide (GO) sheets combined with silk fibroin (scale bar is 600 nm),²³ **h** | SEM image of artificial
 221 hybrid nacre materials with laminated clay-biopolymer composite microplatelets with highly ordered
 222 “brick-and-mortar” arrangement (scale bar is 1 μm),²¹ **i** | AFM image of twisted amyloid fibrillar bundles
 223 (scale bar is 100 nm),²⁴ **j** | SEM image of right-handed helices self-assembled from *D*-cysteine-stabilized
 224 CdTe nanoparticles (scale bar is 100 nm),²⁵ **k** | optical microscopy image of a hierarchically organized

225 cellulose nanocrystal (CNC)-polysaccharide composite with periodic helical organization and sub-micron
226 pitch length (scale bar is 10 μm),²⁶ **I** | AFM image of silica deposited protein core-shell nanofilaments (scale
227 bar is 50 nm),²⁷ **m** | SEM image of nanostructured artificial cellulose nanofibrils with anisotropic
228 arrangement visible in fractured areas (scale bar is 200 nm),²⁸ **n** | SEM image of as-spun regenerated
229 silk/CNT fibers (scale bar is 20 μm).²⁹ The hierarchical structure translates into global functions, utilizing
230 a range of time scales and characteristic interactions for each order of magnitude (right hand side).

231

232 **3. Synthetic and bio-inspired materials and structures**

233 In the following, we survey examples of current, state-of-the-art approaches to design, assemble,
234 and understand composite materials with elements of hierarchical organization, followed by a
235 global analysis and categorization of mechanical performance relative to traditional composite
236 classes.

237 **3.1. Shape-morphing composites with ND functionality.** Responsive bio-inspired composites are
238 based upon general principles of creating interfacial stresses, with the inclusion of dynamically
239 responsive elements for active transport, self-healing, touch sensors, tunable photonic structures,
240 and shape morphing observed in nature (Fig. 2 Global Functions bottom panel and Time scale &
241 interactions).³⁰ Volume may change or be conserved in this process, like in sea cucumber
242 (*Holothuroidea*) or Venus flytraps (*Dionaea muscipula*) morphing.³¹ Hierarchical metamaterials
243 utilize both active and passive mechano-functionality in response to external stimuli to achieve
244 ND functionality. Active mechano-functionality, such as muscles or actions that require energy,
245 corresponds to environmental stimuli responses, such as reversible shape transitions or color
246 changes. In turn, passive functionality originates from within biological assemblies. Bonds and
247 molecules can rearrange themselves when exposed to external environmental stimuli while not
248 actively utilizing energy to react. Examples include the sorption-induced bending of wood and the
249 curling of hairs in response to heat.³²

250 One classic example of active bioinspired materials includes dynamic bilayer hydrogels, composed
251 of cellulose fibrils embedded in a soft matrix that enables morphing in wet environments via
252 encoded anisotropic swelling through the pre-programmed fibril orientation.³³ More complex
253 shape transformation (e.g., helicoidal) can be achieved by controlling interfacial stresses in the
254 bilayer structures depending on the swelling ratios and elastic moduli. For example, the aspect
255 ratio of silk bilayer nanosheets can control biaxial stresses and self-rolling into different tubular
256 shapes.³⁴ Engineered structures with pre-programmed elements, sometimes instituted using
257 kirigami/origami, can show organized transformations due to complex buckling and adaptive
258 architectures, and adjust their shapes for complex morphing.³⁵ The so-called 4D behavior with
259 time as additional axis emphasizes the unique, diverse real-time behavior of the structures. This
260 direction in research is explored, for example, in silk-based patches for tympanic membrane
261 repair,³⁶ as well as in soft robotics, which needs special attention beyond the scope of this review.

262 **3.2. Laminated layered composites beyond nacre.** Layered bioinspired materials from graphitic,
263 cellulosic, and other nanomaterials have been produced to mimic and surpass natural nacre
264 composites, in some cases resulting in impressive materials performance and functionalities
265 unseen in traditional laminates (Fig. 2e-h).^{16,37,38} A relatively low volume fraction of reinforcement
266 material in a brick-and-mortar structure can achieve high fracture toughness similar to that of
267 nacre, such as 3.4 $\text{MPa}\cdot\text{m}^{-1/2}$ with 38 wt% clay in PVA composites (comparable to nacre at 4-8

268 MPa m^{1/2}) (Fig. 2f).¹⁵ PVA hereby increases the composite's energy dissipation. Tougher materials
269 have been designed by alternatively stacking microplatelets with similar dimensions to those of
270 aragonite used in nacre between thick chitosan layers.^{39,40} Microplatelets can be decorated by
271 nanoparticles and sintered to adjust the size of asperities and mineral bridges, facilitating resistance
272 to sliding (Fig. 2f-h and Global Functions, top two panels). Engineering of non-platelet functional
273 particles, including hydroxyapatite⁴¹ and zirconia polycrystals,⁴² might involve rotation for energy
274 dissipation as a toughening mechanism.⁴³

275 A strong interface is critical for effective load transfer and energy dissipation as demonstrated in
276 the early studies using layer-by-layer assembled composites; however, the interface also needs to
277 be compliant to deflect cracks and delocalization stresses. The complementary pairing of polymers
278 with inorganic fillers is characterized by the superposition of multiple types of interfacial
279 interactions that differ in strength and dynamics. Adding polymers to control relaxation dynamics
280 is considered an effective toughening method.^{22,37} Exceptional values in strength and modulus can
281 be achieved in composites with high inorganic phase content (above 90%), contributing to stiffness
282 that increases intrinsic toughening via crack deflection. Necessary interfacial interactions can be
283 tailored via nanosized building blocks during biomineralization.^{38,42} An aspect that has often been
284 overlooked is the biochemistry of proteins that serve as essential building blocks or templates that
285 accurately regulate biomineralization. For instance, with recent advances in RNA sequencing and
286 high-throughput proteomics techniques, one can reliably design full-length sequences that bear
287 additional reinforcement potential.⁴⁴

288 In another high-performance synthetic nacre, the interlayer polymer is a blend of a chitin/silk
289 fibroin matrix and acidic proteins, which provides a robust interface and a unique interlocking
290 mechanism while facilitating large shear deformation and strain hardening in the polymeric
291 phase.⁴⁵ In this manner, the combination of nanofibrous materials with 2D nanosheets is an
292 efficient option for synergistic strengthening.⁴⁶ A recent breakthrough involves the design of
293 interfaces that enable large-scale sliding of tablets in engraved glass laminations, leading to up to
294 more than double the toughness of tempered soda-lime glass and more than triple the toughness of
295 PMMA (plexiglass).⁴⁷ The uniform plate geometry and patterning avoid strain localization and
296 maximize energy dissipation. However, at the next level of hierarchy, additional complexity like
297 symmetry-breaking alignment and correlated twisting in stacks must be introduced to enhance
298 mechanical performance.

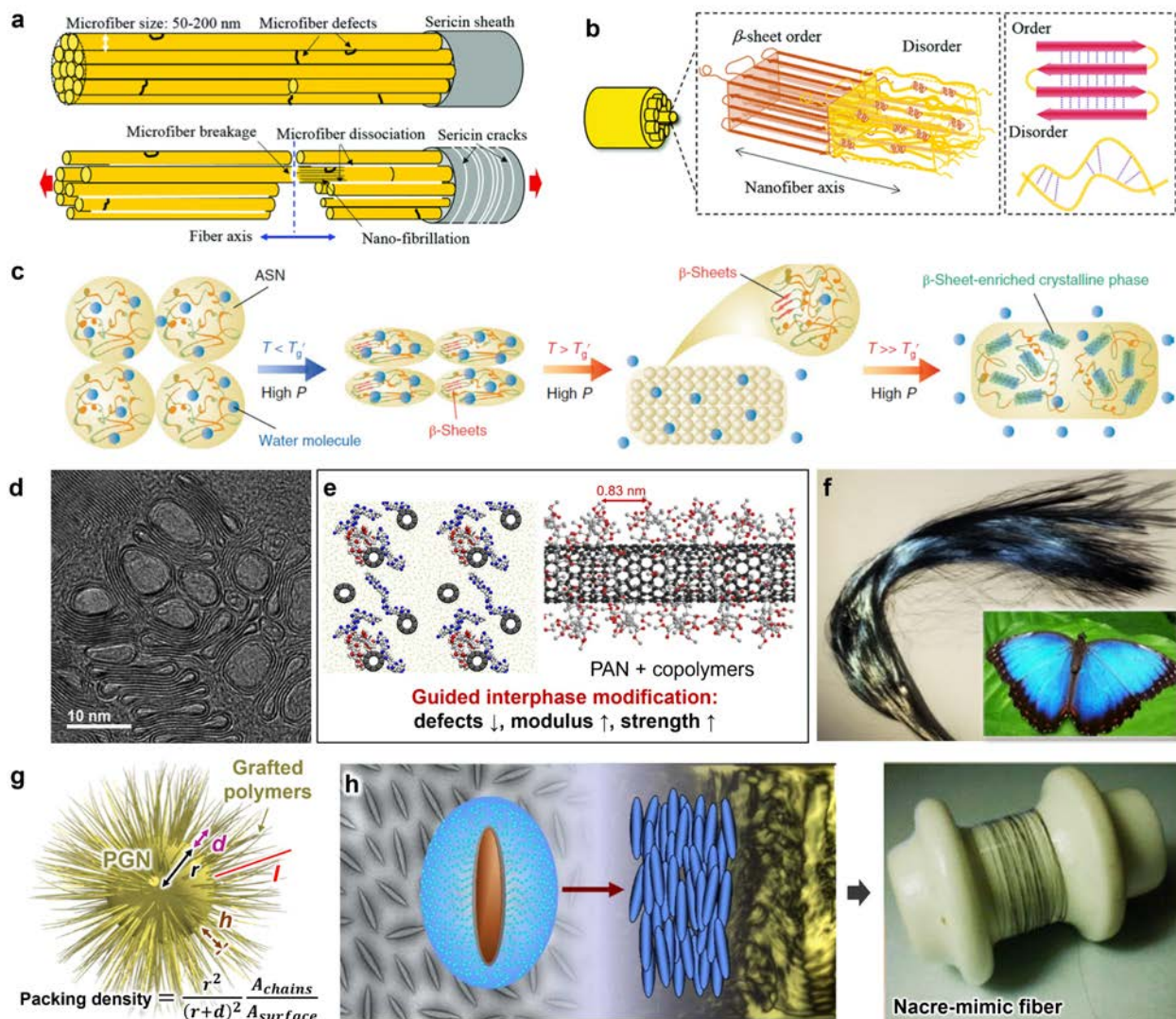
299 **3.3. Twisted laminated Bouligand and chiral composites.** Another class of laminated materials
300 features organized twisted stacking with a slight rotation and twisting angle per layer, commonly
301 referred to as Bouligand structure (Fig. 2d).^{48,49} As seen in mollusk shells and arapaima fish scales
302 in nature, these twisted hierarchical structures demonstrate a remarkable strength and toughness to
303 resist compression and penetration damage.⁵⁰ The unusual toughening mechanism arises from
304 multiple layers in the hierarchical architecture. For example, a mineralization gradient created by
305 a helicoidal arrangement in a herringbone superstructure deflects and twists crack propagation.
306 The striated region consists of circumferentially oriented fibers and exhibits impressive
307 compression during impact and exceptional toughness during stretching.⁵¹ Furthermore, double-
308 Bouligand structures have been found to support mechanical robustness, for example, in the
309 stomatopod dactyl club.⁵²

310 These superstructures with unusual performance are a great inspiration for synthetic hierarchical
311 chiral and twisted materials. Various top-down micro/nanofabrication techniques have been

312 explored, including electrochemical deposition and direct laser writing.⁵³ Precise control of
313 hierarchical structures from the nanoscale to the macro-scale and large-scale fabrication are still a
314 challenge, however. Hereby, bottom-up strategies using directed assembly of individual entities
315 could provide a faster solution. Better precision at the local level was achieved by controlling the
316 surface chemistry, geometry, and dimensions that enable fast “construction” of arbitrary
317 geometries and richer possibilities to integrate additional components (Figure 2i-k).⁵⁴ Traditional
318 liquid crystals (LC) with chiral nematic (cholesteric) phases can be applied as templates, and a
319 well-known example is the organization of polysaccharide nanocrystals, such as cellulose
320 nanocrystals (CNCs) and chitin nanocrystals (ChNCs) derived from plants and crustaceans,
321 respectively, into chiral nematic lyotropic LC phases.^{55,56} Transparent films made from mixtures
322 of wood and CNCs nanocrystals have reached strength similar to that of bone,¹⁶ and helical
323 organization in CNCs leads to selective color reflection of circularly polarized light (Fig. 2k).⁵⁷
324 Switchable lasers, controlled by relative humidity, have been recently built from plant-based CNCs
325 and fluorescent polymers at room temperature.⁵⁸

326 *In silico* studies of the behavior of the Bouligand shell and thin film structures reveal a multitude
327 of mechanisms for coping with mechanical impact.⁵² Depending on fiber material properties,
328 Bouligand structures can result in band gaps that promote impact tolerance and facilitate the
329 propagation of deformation waves, resulting in energy redirection and better performance at high
330 strain rates. Experiments demonstrated crack twisting and distributed damage mechanisms with
331 greater energy dissipation due to the minute differences in fiber orientation and reduced
332 delamination. Twisted laminated structures drive the crack path in tortuous trajectories around
333 designed heterogeneities.^{50,59} These techniques found in nature are applied in engineered
334 heterogeneous materials, like some types of ceramics and ballistic armor, that drive the crack path
335 in tortuous trajectories governed by heterogeneities. The functionality of Bouligand structures
336 finds uses in optics, acoustics, and mechanics; however, current synthetic structural composites
337 are not commonly tough unlike silks and other fibrous composites.

338 **3.4. Fibrous and hairy nanoparticle composites.** Fibrous composites are among the most
339 sophisticated hierarchical structures in nature (Fig. 2a, b, l-m, Fig. 3). Silk, keratin, cartilage, and
340 basal membranes are examples of an extraordinary class of natural nanomaterials that exhibit
341 unparalleled mechanical performance and additional functionalities, such as ion-selectivity
342 essential for applications in numerous energy technologies.⁶⁰⁻⁶² Silks from spiders’ webs and
343 cocoons have a wide variety of functions, ranging from absorption of the kinetic energy (spiders’
344 webs) to the protection of larva (hard cocoon), and exhibit an increase in toughness at high
345 deformation rate⁶⁰ and at cryogenic temperatures.⁶¹ These unique combinations are possible due
346 to the multi-domain architecture of silk proteins that control the energy dissipation mechanisms.
347 Enhanced toughening in silks is governed by the stiffening mechanism of the individual fibrils
348 with increased friction between them, resulting in resistive slippage and diverting crack growth
349 (Fig. 3a),⁶¹ akin to morphologies in CNT fibers.⁶³ Further toughening mechanisms observed in
350 fiber composites include fiber pullout and fiber bridging, contributing to increased fracture
351 toughness. At the molecular level, intrinsic toughening is linked to nanofibrils with a high degree
352 of alignment (Fig. 3b). Furthermore, amorphous silk can convert into highly crystalline silk (Fig.
353 3c) by processing at temperatures above T_g , resulting in exceptional self-reinforced material
354 properties.⁶⁴
355



356
 357 **Figure 3 | Fiber-based composites.** **a** | Schematic representation of the microfibrils from *A. pernyi* silk (top)
 358 and the deflected fracture path that originated from a crack on the interface between sericin and the silk
 359 core (bottom).⁶¹ **b** | The hierarchical structure of *A. pernyi* silk fiber. **c** | A proposed mechanism for the
 360 structural transition of regenerated amorphous silk during thermal processing.⁶⁴ **d** | TEM images of CNT
 361 based composites and carbon fiber.⁶⁵ **e** | Interphase modification through helically ordered wrapping of
 362 PMMA as well as of other polymers around single-walled CNTs increases alignment, modulus, and
 363 strength.^{66,67} **f** | Surface-modified carbon fibers in polymer matrix demonstrating blue structural color.⁶⁸ **g** |
 364 The general scheme of polymer-grafted nanoparticles.⁶⁹ For a local radius of curvature of the particle r ,
 365 the packing density of the polymer chains decreases for an increased, arbitrary distance d from the surface. The
 366 effective thickness of the polymer h is shorter than the extended chain length l and influences the interfacial
 367 properties. Inclusion of solvent and interdigitation with neighbor nanoparticles controls the toughening
 368 mechanism. **h** | An example of self-assembly of polymer-grafted hairy nanoparticles into fibers. The
 369 background (left) shows a TEM image of films of silica-coated α -Fe₂O₃ rods end-grafted with PMMA
 370 brushes,⁷⁰ which self-assemble in a good solvent such as toluene to form lyotropic nematic LCs as seen
 371 from polarized optical microscopy (right). The LC phases are enabled by tight control of the microstructures
 372 in PGN/polymer composites and facilitate spinning fibers with control over hierarchical architectures,
 373 dramatically enhancing both structural and functional properties. Similar processes are used to graft PAN

374 to graphene oxide nanoparticles, using a precursor to spin nacre-mimetic fiber.⁷¹ 2D materials such as
375 graphene and MXenes,⁷² or highly aligned 1D CNTs and CNCs with grafted polymers can also form
376 functional fibers with properties depending on nanoparticle chemistry and shape.

377 Beyond natural fibers, carbon fibers are examples of ultra-strong and tough materials that exhibit
378 exceptional modulus and strength per unit mass that places them in a special parametric space
379 rarely achieved by other composites (Fig. 3d-f). Their current best performance stands at around
380 400 GPa modulus and 8 GPa tensile strength, while the theoretical limits remain at approximately
381 1000 GPa and 100 GPa, respectively.⁷³ Engineering the alignment of carbon nanotubes (CNTs)
382 and polymer gel precursors as well as controlling defect formation is necessary to facilitate
383 improvements (Fig. 3d, e).^{66,67} For example, precisely tailored interfacial properties in CNT-
384 polymer nanocomposites with polymethyl methacrylate (PMMA)-modified CNTs show up to 5x
385 increase in tensile modulus and ~3x increase in tensile strength.⁷⁴ The inhomogeneity of carbon
386 fiber surfaces also causes sp² and sp³ carbon hybridization, which has been exploited to create *in-*
387 *situ* polymerized hierarchical structures that exhibit structural color like that of butterfly wings
388 (Fig. 3f).^{30,68}

389 A new generation of synthetic composites involves polymer-grafted hairy nanoparticles (PGNs)
390 (Fig. 3g, h).⁷⁵ PGNs are core-shell particles, where inorganic nanoparticle cores such as spheres,
391 cubes, cones, rods, or sheets are directly linked with a shell of polymer chains using covalent or
392 nonbonded interactions (Box 1a-d).⁶⁹ These core-shell architectures offer unprecedented
393 opportunities to precision-tailor interphases. The volume fraction of the PGNs and the packing
394 density of the grafted polymer chains can be controlled, including as a function of distance from
395 curved nanoparticle surfaces, and entanglements with the polymer matrix control the toughening
396 mechanism.⁷⁶ Particles with congruent geometry but having stiff spikes that replicate pollen and
397 viruses also show unusual properties represented by anomalously high resistance against
398 agglomeration and responsive behavior, as discussed in the next section.

399 **3.5. Transcending design across different materials classes.** The selected examples of materials
400 designs discussed above cannot reflect the rich variety of this field. We compare the enormous
401 range of multifunctional attributes and mechanical properties realized in bioinspired composites
402 to traditional engineering composites in the same parametric space in two corresponding Ashby
403 plots (Fig. 4 and Table 1). The analyzed composites are color-coded according to their origin
404 (biological or synthetic materials), type of morphologies (nacre-like, twisted, disordered, and
405 cylindrical, fibrous microstructures), as well as parametric space occupied by traditional materials
406 classes: ceramics, elastomers, metals, and fibrous composites (gray circles in Fig. 4).

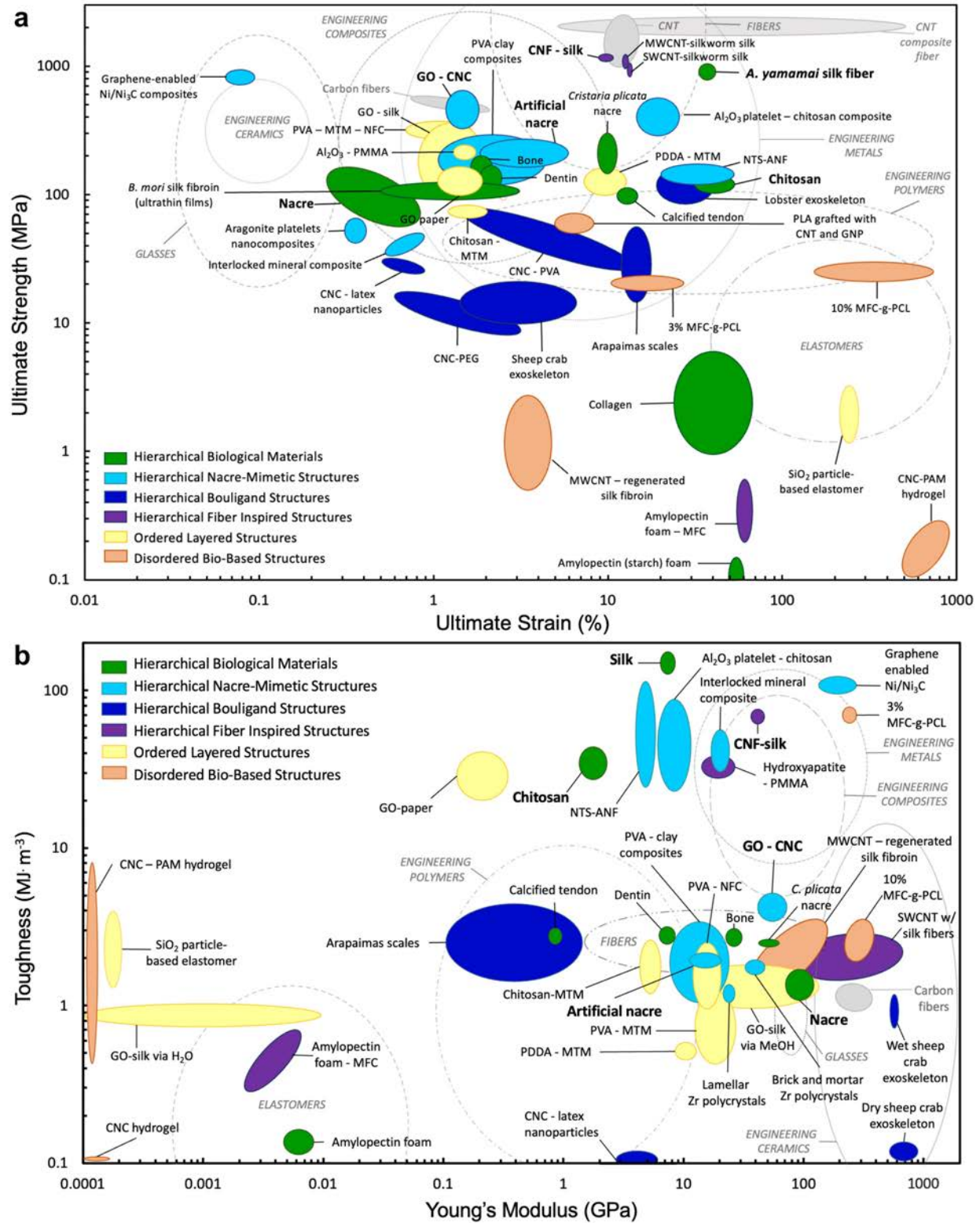
407 Many engineering materials like carbon fiber polymer composites achieve high strength and
408 stiffness, while aluminum has a lower strength and stiffness but high toughness and ductility.³
409 When analyzing available materials data in terms of mechanical strength and elasticity (ultimate
410 strength vs. ultimate strain), which is vital for practical designs of very strong materials with high
411 resilience and non-brittle failure, we observe that known bio-inspired composites mostly occupy
412 the same parametric space as traditional composite materials (Fig. 4a). The majority of known
413 bioinspired composites with soft components such as CNT-silk and PVA-montmorillonite clay
414 (MTM)-nano fibrillated cellulose (NFC) composites are comparable in ultimate strength to
415 common engineered ceramics, polymers, and metals (~0.1 - 1 GPa) (Fig. 4a). Thereby, the strength
416 of mineral or ceramic components, as well as that of the polymers can vary. The softer components,

417 reconfigurable interfaces, and gradient organization facilitate higher deformability than synthetic
418 composites, including maximum strains of 10%, and their ability to reconfigure from planar to
419 highly curved or wrinkled, resulting in dynamic morphing.^{34,69,75,76}

420 The strength of existing biological and bioinspired composites can match advanced synthetic fiber-
421 based composites, e.g., when silks, keratins, and aramid nanofibers (ANFs) are combined with
422 carbon nanotubes.^{14,77} Beyond the elastic regime, yielding and strain hardening can result from
423 local rearrangements such as disentanglement, strain-induced crystallinity, and chain slippage.
424 Such processes add significant plasticity and result in ultimate strains of hundreds of percent. The
425 combination of high ultimate strains with high strength in some wood-keratin composites
426 sometimes surpasses that reported for synthetic fibrous composites (Fig. 4a). Second, if
427 mechanical performance is considered in terms of toughness vs. stiffness (Young's modulus),
428 biological and bio-derived composites (*i.e.*, those utilizing some quantity of natural materials) also
429 perform like traditional composites (Fig. 4b). Bio-inspired composites dramatically extend the
430 parametric space towards extremely compliant materials with uniquely combined high toughness
431 and modulus, comparable to engineering polymers and ceramics (Fig. 4b). Some of these bio-
432 inspired materials occupy valuable, non-traditional parametric space with extreme toughness, up
433 to 100 MPa/m³ for silk, chitosan, and wood-based composites, as well as high elastic moduli up to
434 tens of GPa (Fig. 4b). Bioinspired composites can perform much better than regular
435 elastomers/gels, showing high toughness values up to 10 MPa/m³ (Fig. 4b). Specifically, silk-
436 based and ANF-based composites can demonstrate high toughness while not venturing into the
437 standard brittle fracturing regime (Fig. 4b).

438

439



440
 441 Figure 4 | Analysis of mechanical properties of various composites in comparison with natural and
 442 traditional materials classes. Ashby plots comparing a | the ultimate strength vs ultimate strain and b |
 443 the toughness vs Young's modulus for various hierarchical biological materials,^{14,21,39,78-80} nacre-mimetic
 444 structural,^{14,15,21,39,42,46,81-86} Bouligand structural,^{59,87-91} circular hierarchical, fiber inspired

445 structural,^{14,41,77,80,83,84,92} layered ordered composites and random bionanocomposites.^{23,38,39,79,81,84,92-98} The
 446 various strength, strain, toughness (work of fracture), and Young's modulus values are collected from
 447 tensile test data. The hierarchical materials (biological, nacre-mimetic, Bouligand, and cylindrical fibers)
 448 are included in green, light blue, dark blue, and purple, respectively. The ordered layered composites are in
 449 yellow and the random, disordered bio-based structures are included in orange. These materials are
 450 compared against common materials, included in light grey in the background, such as engineering metals
 451 (stainless steel, gold, copper, silver, tin, nickel, various alloys, titanium, Al/Si Carbide, zinc), engineering
 452 polymers (ABS, polycarbonate, polyamide, PEEK, polyethylene, PMMA, PS, PTFE, PVC, POM,
 453 polyester, epoxies, PLA), elastomers (butyl rubber, ethylene vinyl, natural rubber, polychloroprene,
 454 polyurethane, silicone elastomer), fibers (acrylic fiber, aramid fiber, cellulosic fiber, UHMWPE fiber,
 455 polyamide fiber), carbon fiber/carbon nanotubes (CNTs) and CNT composites, engineering ceramics
 456 (alumina, aluminum nitride, boron carbide, silicon carbide, silicon nitride, tungsten carbide, zirconia),
 457 glasses (borosilicate glass, glass ceramic, silica glass, soda glass), and engineering composites.⁹⁹⁻¹⁰¹
 458 Hierarchically structured composites achieve the highest combinations of strength and strain, as well as
 459 toughness and stiffness. Hereby, composites that include biological fibrous components are among the best
 460 performing materials. Hierarchical microstructures imbue unique property combinations via weak and
 461 strong interfaces that improve the performance of soft component composites, as established in earlier
 462 sections, making them comparable to common inorganic engineering materials. High-end fiber-reinforced
 463 composites cannot easily be outperformed in terms of strength and ductility, yet engineering ceramics and
 464 metals like silicon carbide and titanium alloys are outperformed by CNF-silk, SWCNT/MWCNT-silk, and
 465 Al₂O₃-chitosan bio-inspired composites.^{14,39,77} In these examples, exploiting silk's naturally high strength
 466 and ductility while incorporating stiff nanoparticles facilitates an intrinsic toughening mechanism.
 467

468 **Table 1 | Details of the mechanical properties of different materials classes in Figure 4.** The table
 469 includes key mechanical properties for different material types, organized into the same groups and color
 470 codes as the Ashby plots in Figure 4. The categories include (1) hierarchical biological materials, (2)
 471 hierarchical nacre-mimetic materials, (3) hierarchical Bouligand structured materials, (4) hierarchical fiber
 472 inspired materials, (5) ordered, layered structured materials, (6) disordered, bio-based structures that can be
 473 used in common hierarchical materials, and (7) engineering materials. The data points for individual
 474 engineering materials subsets are not further detailed here and can be searched in the *CES Edupack*
 475 database¹⁰⁰ and in the reference by Ashby.⁹⁹ For some materials, the data were not directly reported in
 476 original works and are based on the analysis of tensile data and stress-strain curves using best estimates and
 477 error bars. The designation “~” indicates less certain estimates with high uncertainties.

| Material Type | Material | Ultimate Strength | Ultimate Strain | Toughness | Young's Modulus | Ref |
|-------------------------|---------------------------|-------------------|-----------------|-----------------------|-----------------|-------|
| | | (MPa) | (%) | (MJ·m ⁻³) | (GPa) | |
| Hierarchical Biological | Amylopectin (Starch) Foam | 0.170 ± 0.025 | ~62 | 0.18 | 0.0049 ± 0.0011 | 80 |
| | Bone | 150 | 1.75 | ~2.5 | ~25 | 39 |
| | Calcified Tendon | 80 | 12 | 3.9 | 0.7 | 39 |
| | Chitosan | 108 ± 15 | 42 ± 9 | 32 ± 9 | 1.9 ± 0.3 | 79 |
| | Collagen | 4.2 ± 3.3 | 46 ± 22 | - | 0.025 ± 0.023 | 78 |
| | Dentin | 105 | 2.5 | 2.8 | 7.5 | 39 |
| | Nacre | 95 ± 35 | 0.7 ± 0.5 | 1.8 ± 0.5 | 90 ± 30 | 39,84 |
| <i>C. Plicata</i> Nacre | 172 ± 50 | 0.9 | 2.4 ± 0.5 | 49 ± 11 | 21 | |

| | | | | | | |
|--|--|------------|--------------|-------------|-----------------|-------|
| | A. <i>Yamamai</i> Silk Fiber (Silk) | 875 | 35 | ~150 | ~8.3 | 14 |
| | B. <i>Mori</i> Silk Fibroin | 100 ± 10 | 1.75 ± 1.5 | 0.328 | 7 ± 1 | 78 |
| Hierarchical Nacre-Mimetic | Al ₂ O ₃ Platelet-Chitosan Composite | 315 ± 95 | 21 ± 5 | 41 ± 19 | 10 ± 2 | 39,84 |
| | Aragonite Platelets-Organics Nanocomposites | 64 ± 8 | 0.38 ± 0.07 | - | - | 14 |
| | Artificial Nacre | 267 ± 25 | 4 ± 2 | 2 | 18.6 ± 5 | 21 |
| | Graphene-Enabled Ni/Ni ₃ C Composite | 1022 ± 73 | 0.143 ± 0.02 | 110.2 ± 10 | 222 ± 10 | 85 |
| | Graphene Oxide (GO)-Cellulose Nanocrystal (CNC) Composite | 490 ± 30 | 1.1 ± 0.3 | 3.9 ± 0.5 | 54 ± 7 | 81 |
| | Planar Mineral Composite of Aragonite Films in a Chitosan/Silk Fibroin Matrix | 23 ± 2.8 | ~0.65 | ~8 | ~12 | 86 |
| | Interlocked Mineral Composite of Aragonite Films in a Chitosan/Silk Fibroin Matrix | 43.5 ± 4.5 | ~0.9 | ~30 | ~25 | 86 |
| | Sodium Tetrasilic Mica - Aramid Nanofiber (NTS-ANF) Composites | 130 ± 15 | 50 ± 24 | 67 ± 33 | 4.7 ± 1.7 | 46 |
| | Polyvinyl Alcohol (PVA) - Montmorillonite (MTM) Clay Composites | 170 ± 70 | 2.25 ± 2 | ~1.7 ± 0.6 | 17 ± 9 | 15 |
| | Brick-and-Mortar Zr Polycrystals | - | - | ~1.7 | 42 ± 4 | 42 |
| | Lamellar Zr Polycrystals | - | - | ~1.2 | 29 ± 4 | 42 |
| Hierarchical Bouligand Structures | Arapaimas Scales (Dry and Hydrated) | ~34 ± 17 | ~22 ± 14 | ~3.6 ± 2.4 | ~0.75 ± 0.65 | 59 |
| | CNC-Latex Nanoparticles | 25 ± 4 | 0.7 ± 0.2 | 0.1 ± 0.02 | 3.5 ± 1.5 | 90 |
| | CNC-Polyethylene Glycol (PEG) | ~13.5 ± 4 | ~2.5 ± 2 | - | 1.75 ± 1.25 | 88 |
| | CNC-PVA Composites | 57 ± 12 | 3.75 ± 3.25 | - | ~7.5 ± 4.5 | 89 |
| | Lobster Exoskeleton (Dry, in Parallel and Transverse Directions) | ~145 ± 35 | ~29 ± 16 | - | 4.7 ± 1.6 | 87 |
| | Dry Sheep Crab Exoskeleton | 12.9 ± 1.7 | 1.8 | 0.11 | 764 ± 83 | 91 |
| | Wet Sheep Crab Exoskeleton | 31.5 ± 5.4 | 6.4 ± 1 | 1.02 ± 0.25 | 518 ± 72 | 91 |
| Hierarchical Fiber Inspired Structures | Amylopectin Foam - Microfibrillated Cellulose (MFC) | 0.7 ± 0.25 | 60 ± 3 | ~0.5 ± 0.32 | 0.0046 ± 0.0025 | 80 |
| | Cellulose Nanofibrils (CNF)-Silk Composites | 1050 | 10 | ~65 | ~35 | 14 |
| | Single-Walled Carbon Nanotubes (SWCNT) - Silk Fiber Composite | 5.5 ± 4 | 2.3 ± 1 | ~2.3 ± 1 | 370 ± 300 | 92 |

| | | | | | | |
|---|---|-------------|-------------|----------------|---------------|----------|
| | SWCNT - Silkworm Spun Silk Composite | 785 ± 95 | 13.6 ± 1.2 | 6,600 ± 210 | - | 77 |
| | Multi-Walled CNT (MWCNT)-Silkworm Spun Silk Composite | 925 ± 145 | 15.5 ± 1.3 | 9,000 ± 4,500 | - | 77 |
| Ordered Layered Structures | Al ₂ O ₃ -PMMA (Brick-and-Mortar) | 200 ± 10 | ~1.4 | - | - | 82 |
| | Chitosan-Montmorillonite (MTM) Composite | 81 ± 12 | 1.9 ± 0.6 | 0.9 ± 0.4 | 6.1 ± 0.8 | 79 |
| | GO-Silk Synthesized via H ₂ O | 175 ± 75 | 0.7 ± 0.2 | 0.75 ± 0.25 | 0.005 ± 0.005 | 23 |
| | GO-Silk Synthesized via MeOH | 225 ± 75 | 1 ± 0.4 | 0.8 ± 1.5 | 75 ± 65 | 23 |
| | GO-Paper | 113 ± 9 | 0.3 ± 0.16 | 0.25 ± 0.1 | 32 ± 7 | 84 |
| | PDDA-MTM | 100 ± 10 | 10 ± 2 | ~0.5 | 11 ± 2 | 38,39,79 |
| | PVA-MTM | 150 ± 40 | 0.7 ± 0.2 | ~0.4 | 13 ± 22 | 38 |
| | PVA-MTM Crosslinked with Glutaraldehyde (GA) | 150 ± 40 | 0.33 ± 0.04 | ~0.5 | 106 ± 11 | 38 |
| | PVA-Nanofibrillar Cellulose (NFC) | 223 ± 31 | ~1.25 | 1.46 ± 0.59 | ~15 ± 5 | 96 |
| | PVA-MTM-NFC | 302 ± 12 | ~2 | 3.72 ± 0.63 | 22.8 ± 1.0 | 96 |
| SiO ₂ Particle-Based Elastomer | ~2 ± 1.5 | 270 ± 45 | ~3 ± 2 | 0.002 ± 0.0015 | 94 | |
| Disordered Bio-Based Structures | 3% MFC-G-PCL | 20.5 ± 3 | 450 ± 275 | 73 ± 3.3 | 0.245 ± 0.035 | 97 |
| | 10% MFC-G-PCL | 24 ± 4.2 | 20 ± 5 | 2 ± 1 | 0.280 ± 0.075 | 97 |
| | CNC Hydrogel | ~0.03 | ~250 | ~0.04 | 0.005 | 93 |
| | CNC-PAM Hydrogel | 0.15 ± 0.07 | 716 ± 70 | ~1.6 ± 1 | 0.025 ± 0.007 | 93 |
| | MWCNT-Regenerated Silk Fibroin | ~1.5 ± 1 | ~3.0 ± 0.5 | ~1.9 ± 1.4 | ~0.07 ± 0.05 | 95 |
| | PLA Grafted with CNT and GNP | 66 ± 11 | 6.0 ± 1.1 | - | 2.1 ± 0.5 | 98 |
| Engineering Materials | Elastomers | 27 ± 25 | 610 ± 340 | 0.75 ± 0.45 | 0.024 ± 0.02 | 99,100 |
| | Engineering Ceramics | 550 ± 450 | 0.12 ± 0.6 | 4.5 ± 3.5 | 700 ± 500 | 99,100 |
| | Engineering Composites | 1050 ± 950 | 5.5 ± 5 | 48 ± 43 | 110 ± 95 | 99,100 |
| | Engineering Metals | 1210 ± 1000 | 40 ± 39 | 75 ± 65 | 205 ± 190 | 99,100 |
| | Engineering Polymers | 60 ± 54 | 401 ± 400 | 5.1 ± 5 | 5.1 ± 5 | 99,100 |
| | Fibers | 2000 ± 800 | 19 ± 17.5 | 2.5 ± 0.9 | 70 ± 68 | 99,100 |
| | Carbon Fibers | 680 ± 40 | 1.4 ± 0.6 | 1.05 ± 0.15 | 45 ± 13 | 100 |
| | Carbon Nanotubes (CNT) | 1600 ± 500 | 10 ± 1 | - | - | 100 |
| | CNT Composite Fiber | 1800 | 355 ± 345 | - | 80 | 101 |
| Glasses | 1000 ± 980 | 0.14 ± 0.10 | 1.0 ± 0.5 | 80 ± 20 | 99,100 | |

478

479 Overall, we can conclude that the expansion of characteristics of bioinspired composites into high
480 performance space with extremes beyond traditional metal and ceramic composites is possible,

481 especially if we consider specific features normalized to material density. However, a deeper
482 understanding of the principles behind hierarchical structural and interfacial organization is
483 required.

484 In addition, the characterization of hierarchical materials is challenging and benefits from advances
485 in multiple areas that are not further reviewed here. Critical techniques include scanning probe
486 microscopy (nano-DMA, AFM-IR, AFM-Raman), high-resolution electron microscopy (HR-
487 TEM, STEM, EELS), synchrotron X-ray/neutron scattering, nano-X-ray computed tomography,
488 advanced spectroscopy, as well as *in-situ* real-time monitoring of mechanical properties and
489 dynamic changes in local chemical and morphological features, under ambient conditions, in a
490 fluid environment, and at elevated temperatures.

491

492 **4. Modeling and simulation of hierarchical materials properties**

493 Modeling and simulation of mechanical and other functional properties can guide the design of
494 bioinspired hierarchical structures within an unlimited space of chemistry and assembly across
495 scales. Simulations typically rely on inputs from experimental data, experimentally inspired data,
496 and specific algorithms to calculate sophisticated properties. Knowledge is generated by analyzing
497 the computational results and comparisons to experimental data, extending material screening to
498 hypothetical model structures and property predictions in iterative feedback loops.

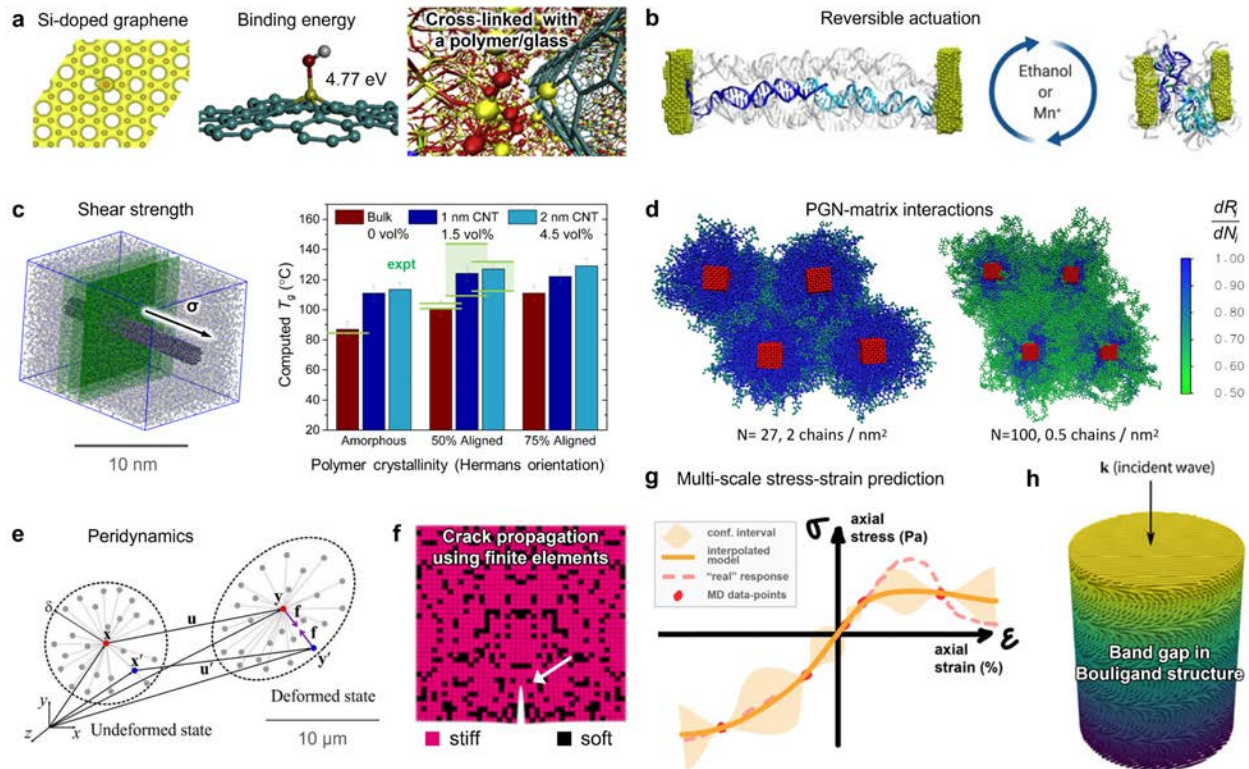
499 Typically, simulations employ individual techniques suitable for specific length scales while the
500 integration across hierarchies remains difficult (Fig. 2).^{102,103} *Ab initio* electronic structure
501 simulations, such as Density-Functional Theory (DFT), are typically used for a few hundred atoms
502 to investigate geometries, transformations in chemical bonding, cohesive energies, band gaps, and
503 elastic moduli, limited to picosecond dynamics and excluding electrolytes. As an example, DFT
504 calculations can forecast the strength of cross-links between fillers and polymer matrices (Fig.
505 5a).¹⁰⁴ The information can then be used to assess the mechanical strength of covalently bonded
506 composites via reactive MD simulations and identify parameters for better reinforcement, such as
507 the diameter of CNTs, the role of defects, and suitable polymer chemistries.¹⁰⁵ At the next level,
508 atomistic Molecular Dynamics (MD) simulations can be applied up to a million atoms and
509 dynamics up to microseconds. Metrics of performance include accurate representations of
510 chemical bonding, the structure (e.g., lattice parameters), surface energies, solvation energies, and
511 mechanical properties (see also Box 1).¹⁰⁶ All-atom MD simulations have explained, for example,
512 up to 80% reversible actuation of β -DNA attached to gold nanoparticles in agreement with
513 experiments on the ~10 nm length scale (Fig. 5b). Structural changes occur in response to the
514 addition of ethanol and variation in the local dielectric constant,¹⁰⁷ as well as upon the addition of
515 multivalent cations that modify the ionic strength.¹⁰⁸ Thermodynamically consistent force fields
516 such as the INTERFACE Force Field¹⁰⁶ allow the analysis of inorganic-(bio)organic materials,
517 including binding energies, interfacial shear strengths, and glass transition temperatures in about
518 ± 5 K agreement with experimental data (Fig. 5c).¹⁰⁹ Effects of conformations, electrolytes, and
519 assembly preferences during processing can be monitored in atomic resolution, which is typically
520 not feasible in experiments and supports the design of MD functional bio-inspired materials.⁶⁶

521 Limitations in the size of all-atom models on the order of 100 nm and in dynamics on the order of
522 1 μ s can be overcome by coarse-grained (CG) simulations, which sacrifice most chemical detail
523 and can explore between 10 to 100 times larger spatial and temporal scales.¹⁰² CG MD simulations

524 have illuminated the role of interphase regions in nanocomposites (Fig. 5d).⁷⁶ In polymer-grafted
525 "hairy" nanoparticles, for instance, a relatively low grafting density and high length of surfactants
526 was shown to enable significant interdigitation of the modified nanoparticles and improvements in
527 mechanical properties (Fig. 5d).^{75,76} MD and CG methods also uncover scaling relations and
528 provide data to train ML algorithms for accelerated property predictions (Box 2).¹¹⁰ At scales
529 beyond micrometers, the mechanical response of composite materials can be effectively analyzed
530 using peridynamics simulations, phase field models, and the finite element method (FEM).¹¹¹
531 Peridynamics models involve bonds inside the material and mimic associated deformations (Fig.
532 5e).¹¹² Peridynamics is well suited to simulate heterogeneous fracture evolution of polymers,
533 including elastic and plastic deformation, unguided crack nucleation and growth, and crack
534 branching at interfaces. Alternatively, phase-field models can be employed which assume a
535 continuum representation and a specific parameter that represents the progress of fracture at every
536 point in the specimen. FEM simulations of fracture can be challenging due to the presence of
537 ubiquitous matrix/inclusion interfaces and complex geometries that defy the underlying continuum
538 assumptions. Hereby, atomistically-informed FEM simulations can overcome some of these
539 challenges (Fig. 5f, g)¹¹³ and have been helpful, for example, to analyze crack twisting and
540 distributed damage mechanisms in Bouligand structures to explain increased energy dissipation
541 before failure and promote impact tolerance.¹¹⁴ Band gaps and wave filtering capabilities could
542 also be identified as a function of the fiber material and orientation (Fig. 5h).

543 In summary, routine simulations are currently feasible in selected areas on the time-length
544 continuum and provide guidance on specific aspects of composites (Fig. 2, right column). Some
545 methods are also frequently used in combination (MD/DFT, CG/atomistic MD, FEM/MD).^{102,111}
546 Grand challenges include better representation of structure-function phenomena across different
547 length scales and new approaches to predict the behavior over long-time scales. Fracture
548 mechanisms of bio-based materials are largely an open field as they have been far less studied than
549 those of less heterogeneous materials. Specifically, the prediction of tortuous fracture in combined
550 soft and hard material components remains a very challenging problem.

551



552
 553 **Figure 5 | Insights into the function and mechanics of bioinspired composites by modeling and**
 554 **simulation.** **a** | Electronic structure of local Si-defects in graphene and calculation of a C-SiH bond energy
 555 using DFT. Subsequent all-atom MD simulations of cross-linking on CNT surfaces can guide experiments
 556 to optimize bonding to polymer matrices.^{104,105} **b** | Functionalization and up to 80% reversible actuation of
 557 gold nanostructures modified with DNA, induced by changes in solvent or ionic concentration according
 558 to all-atom MD simulation.^{107,108} **c** | MD simulations of shear strength and glass transitions in PAN/CNT
 559 composites. Glass transition temperatures reveal ± 5 K agreement with experimental data. The molecular
 560 origin of T_g , the influence of CNT bundling and of CNT volume fraction could be identified.¹⁰⁹ **d** | Hairy
 561 nanoparticles support non-covalent mixing with a polymer matrix (green), whereby the packing density and
 562 chain length of the “hairy surfactants” (blue) has a critical influence on the composite properties, shown by
 563 coarse-grain MD simulations.⁷⁶ With the advancement of reliable all-atom force fields¹⁰⁶ and larger-scale
 564 coarse-grain models,¹¹¹ it is possible to predict the role of nano- and microscale features such as packing,
 565 defects, and interfaces on macroscale properties. **e** | In peridynamics, bond lengths and bond failure are
 566 monitored to compute continuous deformation and stress-strain characteristics at the microscale. **f** |
 567 Simulation of crack propagation in a FEM simulation (see arrow).¹¹⁵ **g** | Results of multiscale simulation of
 568 the mechanical response of a graphene/epoxy composite. From a large set of data-points from all-atom
 569 simulations and narrowed confidence intervals, Gaussian process regression was used to construct a
 570 surrogate continuum model to predict the stress distribution from the mechanical state (current strain) for
 571 time-independent systems.¹¹³ **h** | Multi-scale simulation of the band gap in Bouligand structures of a
 572 transversely isotropic material using finite elements up to the micrometer scale.¹¹⁴

573
 574

575 **5. Trends, broader impacts, and future developments**

576 Applications of bioinspired composites range from drug delivery, wearable electronics, and
577 human-computer interfaces to structural components for the automotive and aerospace industries.
578 The multifunctional attributes imply a unique combination of properties, including mechanical
579 robustness, flexibility, transparency, sensing, adapting (morphing), optics (photonics), electrical
580 and thermal conductivities.

581 **5.1. Developing ambient bio-synthetic processing techniques.** There is a good, albeit still
582 incomplete, understanding of the fundamental building blocks of biological structures. In most
583 cases, it is still unknown how nature goes from the building blocks to the final, complex
584 hierarchical structure, creating a need to better understand biogenesis or “biofabrication” of
585 materials. There are a few well-studied exceptions, such as the biotechnological production of
586 engineered silk fibers.¹¹⁶ Recent breakthroughs also include understanding of the biofabrication of
587 mussel fiber adhesives¹¹⁷ and of the development of complex hard tissues such as the stomatopod
588 dactyl club (Fig. 2d).⁵¹ However, many intriguing questions remain. For example, the evolutionary
589 principle behind the prevalence of Bouligand structures in biological materials, structure-
590 mechanical property relationships of the twisting angle, and the relative significance of the
591 contribution of material building blocks to the material architecture remain unclear.

592 Amongst novel material design methods, digital manufacturing such as 3D printing combined with
593 advances in artificial intelligence is rising in prominence due to its ability to create highly complex
594 structures. For example, additive biomanufacturing using silk dopes can preserve natural,
595 sustainable, green, and aqueous processes while exploiting new additives, such as aramid
596 nanofibers and other emerging nanofibers from recycled plastics and applications.¹¹⁸ Advances in
597 the addition of other polymers, inorganics, sequestration of bioactive components, the use of
598 microfluidic devices for processing, subtle changes in pH value and electrolyte composition, as
599 well as sampling the space of processing parameters, offer a suite of new options for 3D printing
600 of hierarchical bioinspired materials. Target properties may include, for example, optical clarity,
601 loading with bioactive components, and tunable mechanical performance.

602 Remarkably, all structures discussed here from natural materials are only derived from aqueous-
603 based synthesis and assembly processes conducted at ambient temperature and pressure. When
604 these amazing material outcomes and functional features are considered in the context of using
605 benign conditions to drive material assembly, emulating such systems for our future material needs
606 becomes even more compelling and amplified in importance. New ways to apply environmentally
607 friendly processing as we move to the next generation of processing technologies and bio-inspired
608 material systems would bring enormous benefits in sustainability to our planet.

609 **5.2. Accelerated design using data science and machine learning.** Tremendous innovation and
610 acceleration in precision engineering of nature-inspired materials for targeted functions can be
611 expected by integrating experiments with theory, modeling and simulation, data science, and
612 artificial intelligence tools (Box 2a).¹¹⁵ While structural order at specific length scales has been
613 experimentally demonstrated in synthetic composites, structural hierarchy across multiple length
614 scales remains lacking to-date and may be achieved sooner using such convergent techniques.
615 Simulation and data-driven methods, complemented by mathematical approaches, such as
616 category theory, can link the physiochemical properties, characteristics, and function of a material.

617 The synergy of these approaches introduces a new field of materiomics, which aims at ordering
618 the vast materials space and accelerating materials design in a unified manner (Box 2b, c).^{103,110}

619 Specifically, ML algorithms can accelerate materials discovery as follows.¹¹⁵ Large training sets
620 of data using features of the electronic, atomic, or microscopic scale and known mechanical and
621 other physical properties can be used to train neural networks such as graph neural networks
622 (GNNs) and convolutional neural networks (CNNs) for learning and connecting structure-property
623 relationships.¹¹⁹ The models can then make property predictions for untested structures and help
624 to optimize synthesis and design (Box 2a, b). Novel capabilities in materials design also emerge
625 using graph-theory (GT) based descriptions of nanocomposites, which can capture the networked
626 structure of nanofiber reinforcements.¹²⁰ Concepts from visual art and music have been combined
627 with AI to navigate the vast space of protein sequences.¹²¹ The rapidly growing amount of data
628 from high-throughput experiments and simulations also benefits from the organization in databases
629 and multidimensional analysis with consistent and statistically robust content (Box 2c). A
630 bottleneck is often the extraction of relevant data for a given problem from the literature, which
631 may encompass hundreds of thousands of prior publications and could be accelerated by advances
632 in information retrieval and natural language processing.

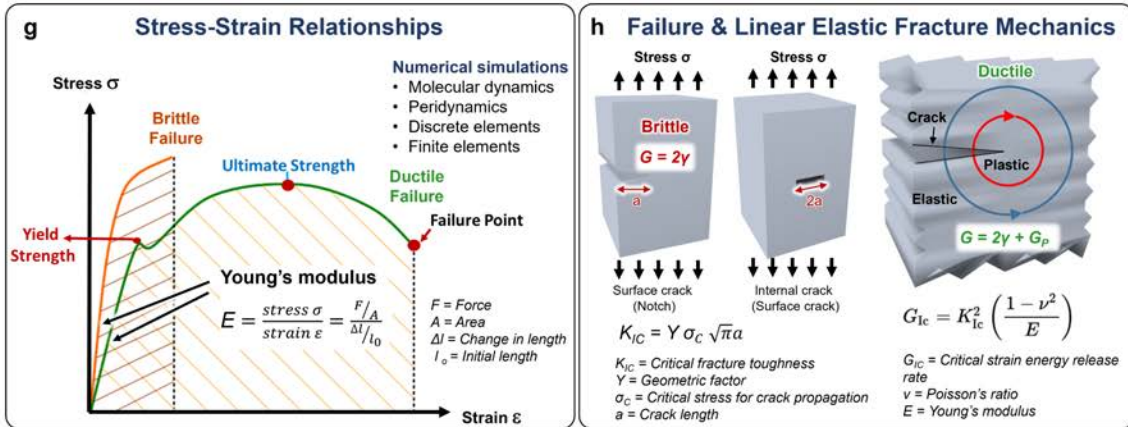
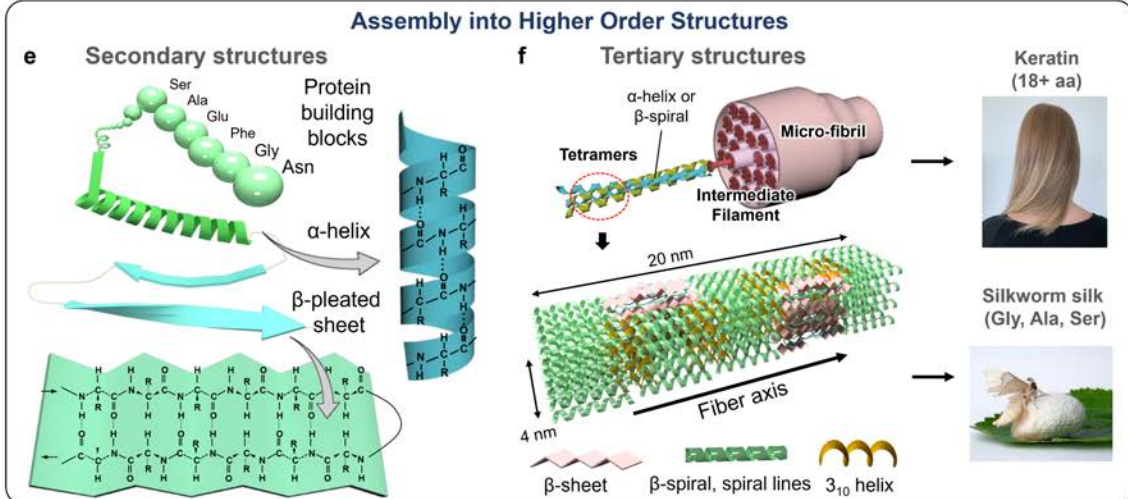
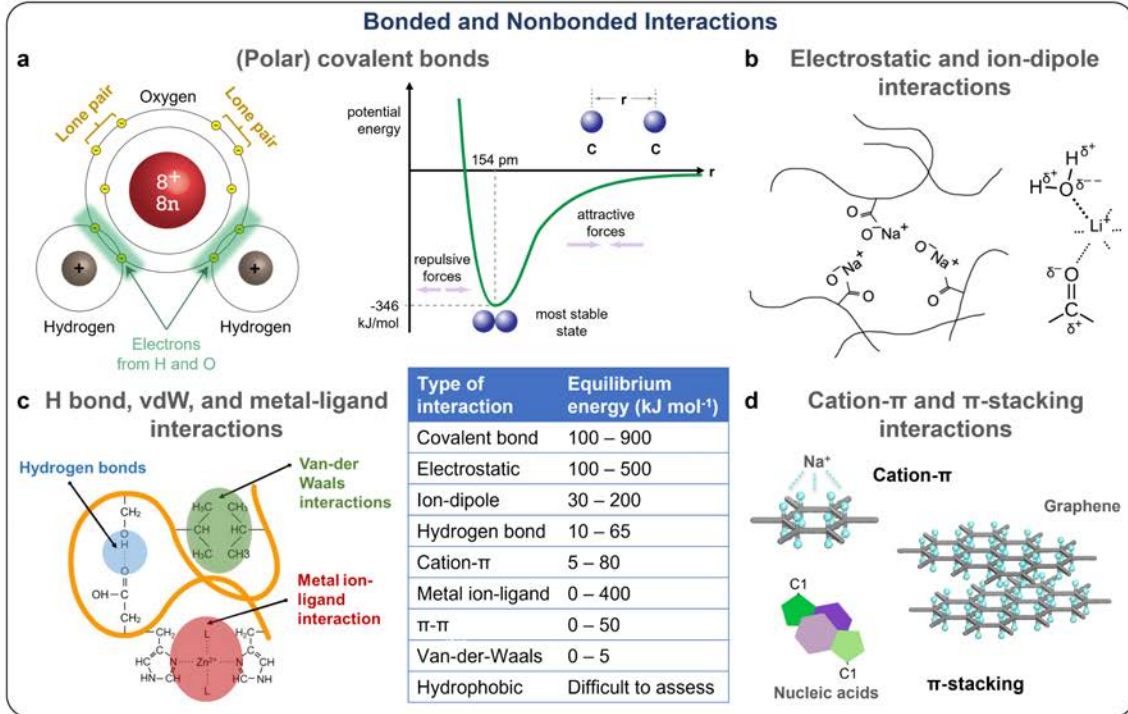
633 Data science also provides tools to better connect high fidelity modeling and simulation across
634 different scales. Specific chemistry knowledge has been precisely translated into nanometer-scale
635 models and force fields to carry out predictive MD simulations.^{103,106} Nevertheless, capturing *any*
636 *new chemistry* and *the effect from the atomic scale to microscale deformation and fracture*
637 *behavior* in models remains a grand challenge. Obstacles involve (1) quickly and accurately
638 parameterizing new chemistry and (2) effectively passing information from atomistic models to
639 coarse-grained models and continuum representations. In addition, uncertainties in experimental
640 nanoscale mechanical characterization of soft materials add complexity in providing guidance and
641 validation for modeling. Data science and machine learning methods are promising to perform the
642 necessary dimensionality reductions of structures and of interaction energies between particles and
643 domains upon entering larger scales (Box 2d).¹²² Such tasks can be achieved in uniform ways by
644 employing hierarchical graph encoders and decoders, whereby chemical identity, geometry, and
645 topological patterns play a critical role, similar to those explored earlier for multiscale simulations
646 in adaptive resolution.¹⁰² ML techniques may also be adjusted to enforce certain principles such
647 as a Hamiltonian system if used to substitute physics-based simulations. Community-wide efforts
648 to standardize reference states, key properties for validation, protocols for simulations, and open
649 documentation of ML algorithms would enhance reproducible usage and integration of
650 computational methods by the experimental community.

651 **5.3. Future trends and impact.** Nature is highly efficient in designing materials with unique optical,
652 mechanical, and other functional property combinations through distinctive processing techniques.
653 The integration of experimental and theoretical work can uncover new classes of bio-inspired
654 materials that can enormously impact society through a unique amalgamation of properties.
655 Modeling techniques including multiscale simulation, AI/ML, and materiomics may reveal hidden
656 opportunities for designing multifunctional materials with high strength and toughness at faster
657 development rates with sustainable routes, increasing the efficiency of material design. However,
658 challenges remain in fulfilling the demand of these bio-inspired composites for high-performance
659 applications such as aerospace composites, where extreme temperature, pressure, and mechanical

660 tolerance are prerequisites. Multiple other functional attributes such as electrical conductivity,
661 optical transparency, morphing, and self-repair could be necessary along with the structural
662 attributes. To-date, the incorporation of nanofillers in bio-inspired hierarchical design with
663 precisely tailored interfaces has shown promise and there is an enormous opportunity for
664 innovation.¹²³

665 Similarly, bio-inspired composites are a treasure for other fields such as biomedical implants and
666 sensors via grafts and engineering, energy storage via lightweight batteries, global sustainability
667 via ambient processing and self-repair, as well as communication and coding via adaptivity and
668 hidden functionalities. In addition, the ambient assembly processes reveal important lessons to
669 emulate in the broader context of materials recycling and upcycling.

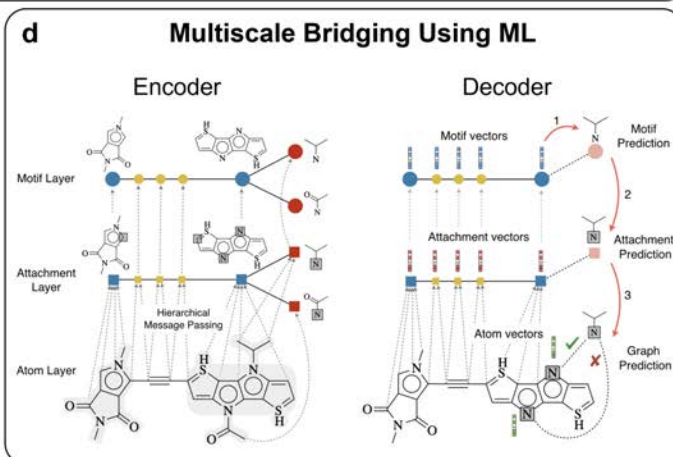
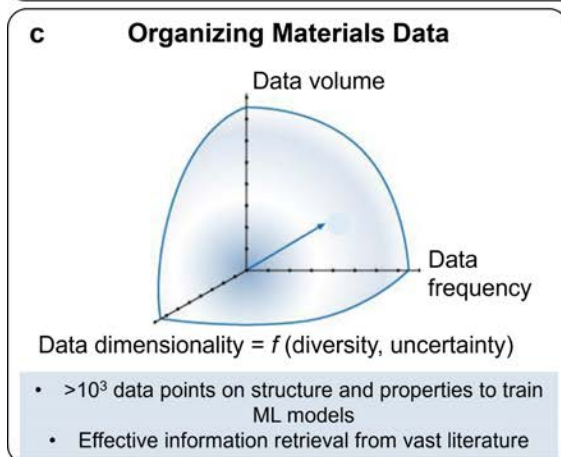
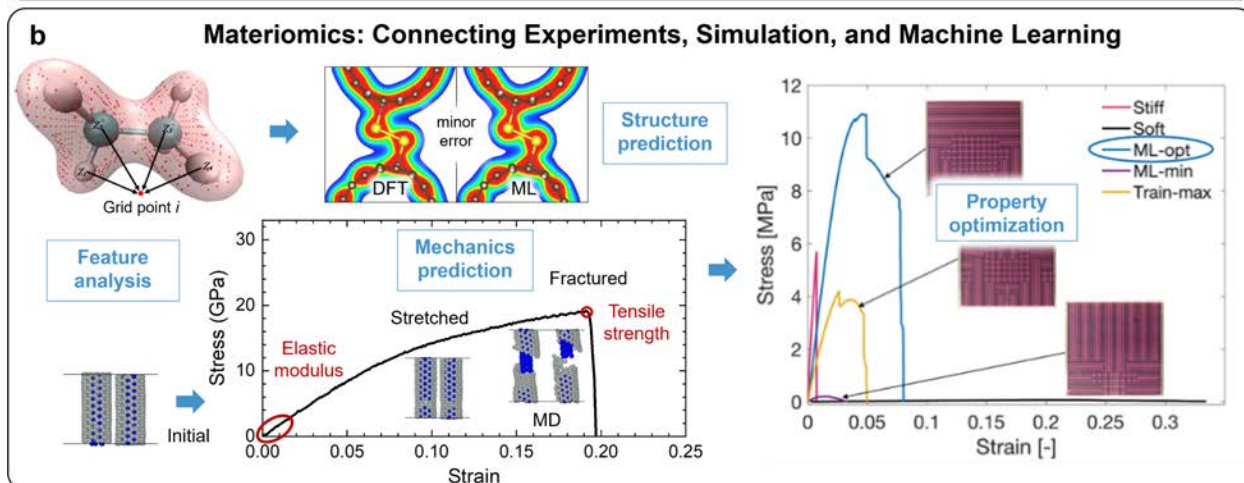
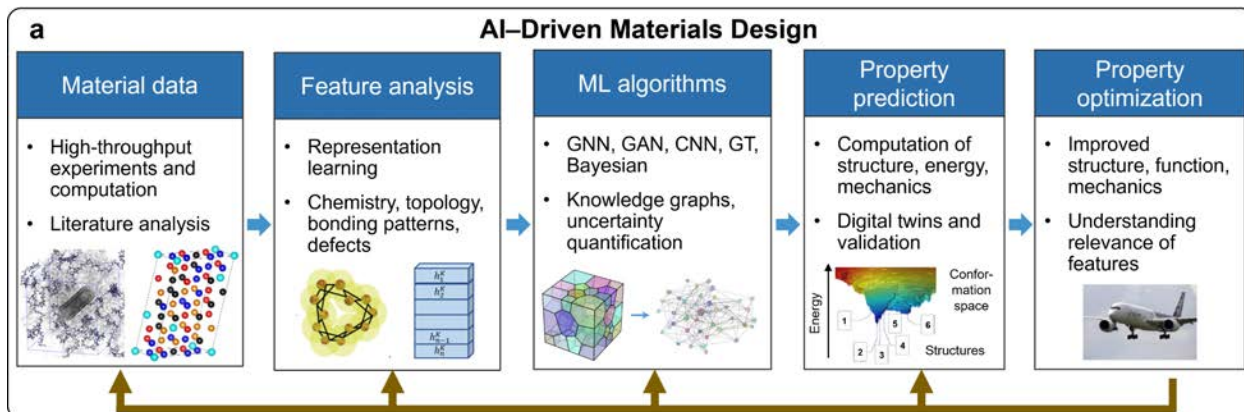
670 Recent developments of laser-grade bio-inspired photonic bandgap materials also showcase the
671 potential for unprecedented applications beyond structural means such as optical communication
672 and adaptive camouflaging. The insights from bioinspired cross-platform approaches answer
673 practically relevant questions such as the high strength of silk, the emergence of disease, the
674 creation of new materials, and the underpinning philosophy of what constitutes a material. The
675 translation among various hierarchical systems poses a new paradigm for elucidating the
676 fundamental biogenic fabrication processes and emergence of advanced properties in materials.
677 Therefore, a new horizon of engineered living materials can provide unique opportunities to create
678 intelligent materials on demand by combining nature and synthetic analogs for self-organizing,
679 self-sustained, self-powered, and self-evolving structures of synthetic living matter.¹²⁴



682 **Box 1 | Fundamentals of interatomic interactions, hierarchical structures, and mechanical behavior.**
683 The primary structure of inorganic and organic compounds is determined by chemical and physical
684 interactions of various strengths (**a-d**).¹²⁵ The molecular structure usually involves covalent bonds of
685 varying polarity as shown for water (**a**, left). The potential energy as a function of distance between two
686 atoms resembles a Morse potential, shown for a C-C single bond (**a**, right). Molecular structures are also
687 influenced by non-covalent interactions such as electrostatic interactions (**b**), hydrogen bonds, van-der-
688 Waals forces, metal-ion ligand (**c**), and π -electron related interactions (**d**). Inter- and intramolecular
689 interactions on the weaker end of the energy spectrum are thermally and mechanically reconfigurable and
690 play a major role in generating cohesion via large numbers across material volumes. The full set of bonded
691 and nonbonded interactions, including specific chemistry and solution conditions such as pH value, directs
692 the folding and assembly of larger molecules and building blocks into higher-order structures (**e** and **f**). For
693 example, the sequence of covalently bonded amino acids and the pattern of hydrogen bonds in proteins
694 determines the formation of random coil, α -helix, β -sheet, and other organized building blocks (**e**). These
695 nanometer-scale building blocks can organize into hierarchical structures such as keratin and silk, including
696 α -helical superhelices in keratin and mechanical stabilization of silk fibrils by β -sheet nanocrystals (**f**).⁸ Key
697 mechanical properties are derived from stress-strain curves, which are obtained by gradually applying a
698 load (stress) to a test sample and measuring the deformation (strain) (**g**). Fracture mechanics analyzes the
699 propagation of cracks and failure in materials (**h**).⁹⁹ Brittle materials fail by crack propagation whereas
700 ductile materials undergo additional plastic deformation, including craze formation in polymers near the
701 crack tip. Crack growth in brittle materials occurs when the increase in surface energy γ of cracks is
702 compensated by a decrease in strain energy via stress release (Griffith theory, total energy for crack growth
703 $G = 2 \gamma$). In ductile materials, the total free energy for crack growth is dominated by plastic deformation G_P
704 and follows the more general Irwin theory ($G = 2 \gamma + G_P$).

705 **End Box 1**

706



707
 708 **Box 2 | Tools needed to further advance the field: AI, materiomics, and multi-scale design.** High
 709 throughput experimentation and machine learning hold great promise to better sample the vast design space
 710 (a). Typically, large amounts of data for one type of systems, about thousands to millions, can be
 711 categorized into features and vector representations for ML analysis. Examples of data sources include high
 712 volumes of X-ray scattering and spectroscopy data, stacks of images from microscopy and tomography, as
 713 well as data from computational structure-property calculations. Thereby, the structural and other physical
 714 data elements need to be supplied together with the corresponding physical properties of interest for
 715 prediction in the entire dataset, i.e., in computer science language, all structural “data” require “labels”, to
 716 be able to build and train an ML algorithm. The algorithm, once trained, can be applied to predict structural,

717 energetic, mechanical, electronic, and other properties for new material structures within and outside the
718 training space. The integration of cutting-edge experimental data into cross-scale simulations and machine
719 learning facilitates a build-measure-learn feedback loop to construct interpretable digital platforms (digital
720 twins) for faster property optimization. As an example, ML of electronic density features from DFT can be
721 used to predict the atomic-scale structure **(b)**. ML of data from MD simulations can predict stress-strain
722 curves for carbon composites with known defects, allowing recommendation of new designs with increased
723 toughness in a feedback loop with experimental data.¹¹⁵ The ever-increasing amount of materials data
724 requires tools for systematic organization, considering data volume, frequency of data generation,
725 dimensionality, and uncertainties **(c)**. Typically, at least thousands of data points are needed to train
726 effective ML models. It is often challenging to retrieve validated information including uncertainties from
727 the rapidly growing number of publications. Hierarchical graph encoders and decoders for molecular
728 structures can be used to accomplish reversible dimensionality reduction to when solving multiscale
729 problems by ML **(d)**.¹²² The approaches have promise to overcome longstanding challenges in multiscale
730 modeling and materials design.

731 **End Box 2**

732

733

734 **Acknowledgements:**

735 The authors would like to acknowledge support from multiple sources: DN - Air Force Office of
736 Scientific Research (AFSOR) 18RXCOR060 and 22RXCOR014, KD - ONR N00014-18-1-2528,
737 MRB - AFOSR FA8650-19-2-5209, MJB - AFOSR FATE MURI FA9550-15-1-0514, LH - Office
738 of Naval Research Global N62909-18-1-2024, SK - PECASE Award ONR N00014-16-1-3175;
739 GCS - Center for Bio-Inspired Energy Sciences (CBES), an Energy Frontiers Research Center
740 (EFRC) under DE-SC0000989, VT - Air Force Research Laboratory FA8650-16-D-5404, AFOSR
741 FA9550-20-1-0305, and NSF-CBET 180349, LCB - AFOSR FA9550-18-1-0381, JAE NSF
742 Career Award CMMI-1454072, PVC - Engineering and Physical Sciences Research Council, grant
743 number EP/R029598/1, HH - NSF 1940335, NSF 1931587, and NASA Space Technology
744 Research Institute STRI-NNX17AJ32G.
745

746 **References**

- 747 1. Wegst, U.G.K., Bai, H., Saiz, E., Tomsia, A.P. & Ritchie, R.O. Bioinspired Structural
748 Materials. *Nat. Mater.* **14**, 23-36 (2015).
- 749 2. Liu, Z.Q., Meyers, M.A., Zhang, Z.F. & Ritchie, R.O. Functional Gradients and
750 Heterogeneities in Biological Materials: Design Principles, Functions, and Bioinspired
751 Applications. *Progr. Mater. Sci.* **88**, 467-498 (2017).
- 752 3. Clancy, A.J., Anthony, D.B. & De Luca, F. Metal Mimics: Lightweight, Strong, and
753 Tough Nanocomposites and Nanomaterial Assemblies. *ACS Appl. Mater. Interfaces*
754 **12**, 15955-15975 (2020).
- 755 4. Ritchie, R.O. The Conflicts Between Strength and Toughness. *Nat. Mater.* **10**, 817-822
756 (2011).
- 757 5. Kotov, N.A., Dekany, I. & Fendler, J.H. Ultrathin Graphite Oxide-Polyelectrolyte
758 Composites Prepared by Self-Assembly: Transition Between Conductive and Non-
759 Conductive States. *Adv. Mater.* **8**, 637-641 (1996).
- 760 6. Huang, W. et al. Multiscale Toughening Mechanisms in Biological Materials and
761 Bioinspired Designs. *Adv. Mater.* **31**, 1901561 (2019).
- 762 7. Tadepalli, S., Slocik, J.M., Gupta, M.K., Naik, R.R. & Singamaneni, S. Bio-Optics and
763 Bio-Inspired Optical Materials. *Chem. Rev.* **117**, 12705-12763 (2017).
- 764 8. Wang, B., Yang, W., McKittrick, J. & Meyers, M.A. Keratin: Structure, Mechanical
765 Properties, Occurrence in Biological Organisms, and Efforts at Bioinspiration. *Progr.*
766 *Mater. Sci.* **76**, 229-318 (2016).
- 767 9. Chen, M.L. et al. The Hierarchical Structure and Mechanical Performance of a Natural
768 Nanocomposite Material: The Turtle Shell. *Coll. Surf. a-Physicochem. Eng. Aspects*
769 **520**, 97-104 (2017).
- 770 10. Hieronymus, T.L., Witmer, L.M. & Ridgely, R.C. Structure of White Rhinoceros
771 (*Ceratotherium simum*) Horn Investigated by X-ray Computed Tomography and
772 Histology With Implications for Growth and External Form. *J. Morphology* **267**, 1172-
773 1176 (2006).
- 774 11. Teyssier, J., Saenko, S.V., van der Marel, D. & Milinkovitch, M.C. Photonic Crystals
775 Cause Active Colour Change in Chameleons. *Nat. Commun.* **6**, 6368 (2015).
- 776 12. Huang, W. et al. A Natural Energy Absorbent Polymer Composite: The Equine Hoof
777 Wall. *Acta Biomater.* **90**, 267-277 (2019).
- 778 13. Chon, M.J. et al. Lamellae Spatial Distribution Modulates Fracture Behavior and
779 Toughness of African Pangolin Scales. *J. Mech. Behav. Biomed. Mater.* **76**, 30-37
780 (2017).
- 781 14. Ren, J. et al. Biological Material Interfaces as Inspiration for Mechanical and Optical
782 Material Designs. *Chem. Rev.* **119**, 12279-12336 (2019).
- 783 15. Morits, M. et al. Toughness and Fracture Properties in Nacre-Mimetic Clay/Polymer
784 Nanocomposites. *Adv. Funct. Mater.* **27**, 1605378 (2017).
- 785 16. Natarajan, B. & Gilman, J. Bioinspired Bouligand Cellulose Nanocrystal Composites:
786 A Review of Mechanical Properties. *Philos. Trans. A Math. Phys. Eng. Sci.* **376**,
787 20170050 (2018).
- 788 17. Grant, A.M. et al. Silk Fibroin-Substrate Interactions at Heterogeneous Nanocomposite
789 Interfaces. *Adv. Funct. Mater.* **26**, 6380-6392 (2016).
- 790 18. Wang, Q. et al. Observations of 3 nm Silk Nanofibrils Exfoliated from Natural
791 Silkworm Silk Fibers. *ACS Mater. Lett.* **2**, 153-160 (2020).

- 792 19. Shao, Z.Z. & Vollrath, F. Surprising Strength of Silkworm Silk. *Nature* **418**, 741-741
793 (2002).
- 794 20. Guarin-Zapata, N., Gomez, J., Yaraghi, N., Kisailus, D. & Zavattieri, P.D. Shear Wave
795 Filtering in Naturally-occurring Bouligand Structures. *Acta Biomater.* **23**, 11-20
796 (2015).
- 797 21. Gao, H.L. et al. Mass Production of Bulk Artificial Nacre with Excellent Mechanical
798 Properties. *Nat. Comm.* **8**, 287 (2017).
- 799 22. Das, P. et al. Nacre-mimetics with Synthetic Nanoclays up to Ultrahigh Aspect Ratios.
800 *Nat. Commun.* **6**, 5967 (2015).
- 801 23. Hu, K., Gupta, M.K., Kulkarni, D.D. & Tsukruk, V.V. Ultra-Robust Graphene Oxide-
802 Silk Fibroin Nanocomposite Membranes. *Adv. Mater.* **25**, 2301-2307 (2013).
- 803 24. Adamcik, J. et al. Measurement of Intrinsic Properties of Amyloid Fibrils by the Peak
804 Force QNM Method. *Nanoscale* **4**, 4426-4429 (2012).
- 805 25. Feng, W.C. et al. Assembly of Mesoscale Helices with Near-unity Enantiomeric
806 Excess and Light-Matter Interactions for Chiral Semiconductors. *Sci. Adv.* **3**, e1601159
807 (2017).
- 808 26. Adstedt, K. et al. Chiral Cellulose Nanocrystals with Intercalated Amorphous
809 Polysaccharides for Controlled Iridescence and Enhanced Mechanics. *Adv. Funct.*
810 *Mater.* **30**, 2003597 (2020).
- 811 27. Cao, Y.P., Bolisetty, S., Wolfisberg, G., Adamcik, J. & Mezzenga, R. Amyloid Fibril-
812 directed Synthesis of Silica Core-Shell Nanofilaments, Gels, and Aerogels. *Proc. Natl.*
813 *Acad. Sci. U. S. A.* **116**, 4012-4017 (2019).
- 814 28. Mittal, N. et al. Multiscale Control of Nanocellulose Assembly: Transferring
815 Remarkable Nanoscale Fibril Mechanics to Macroscale Fibers. *ACS Nano* **12**, 6378-
816 6388 (2018).
- 817 29. Ling, S. et al. Polymorphic Regenerated Silk Fibers Assembled Through Bioinspired
818 Spinning. *Nat. Comm.* **8**, 1387 (2017).
- 819 30. Zhao, Q.L., Wang, Y.L., Cui, H.Q. & Du, X.M. Bio-Inspired Sensing and Actuating
820 Materials. *J. Mater. Chem. C* **7**, 6493-6511 (2019).
- 821 31. de Espinosa, L.M., Meesorn, W., Moatsou, D. & Weder, C. Bioinspired Polymer
822 Systems with Stimuli-Responsive Mechanical Properties. *Chem. Rev.* **117**, 12851-
823 12892 (2017).
- 824 32. Egan, P., Sinko, R., LeDuc, P.R. & Keten, S. The Role of Mechanics in Biological and
825 Bio-Inspired Systems. *Nat. Commun.* **6**, 7418 (2015).
- 826 33. Gladman, A.S., Matsumoto, E.A., Nuzzo, R.G., Mahadevan, L. & Lewis, J.A.
827 Biomimetic 4D Printing. *Nat. Mater.* **15**, 413-418 (2016).
- 828 34. Ye, C.H. et al. Bimorph Silk Microsheets with Programmable Actuating Behavior:
829 Experimental Analysis and Computer Simulations. *ACS Appl. Mater. Interfaces* **8**,
830 17694-17706 (2016).
- 831 35. Zhang, Y.H. et al. A Mechanically Driven Form of Kirigami as a Route to 3D
832 Mesostructures in Micro/Nanomembranes. *Proc. Natl. Acad. Sci. U. S. A.* **112**, 11757-
833 11764 (2015).
- 834 36. Lee, J.H., Lee, J.S., Kim, D.K., Park, C.H. & Lee, H.R. Clinical Outcomes of Silk
835 Patch in Acute Tympanic Membrane Perforation. *Clin. Exp. Otorhinolaryngol.* **8**, 117-
836 122 (2015).

- 837 37. Zhao, C. et al. Layered Nanocomposites by Shear-Flow-Induced Alignment of
838 Nanosheets. *Nature* **580**, 210-215 (2020).
- 839 38. Podsiadlo, P. et al. Ultrastrong and Stiff Layered Polymer Nanocomposites. *Science*
840 **318**, 80-83 (2007).
- 841 39. Bonderer, L.J., Studart, A.R. & Gauckler, L.J. Bioinspired Design and Assembly of
842 Platelet Reinforced Polymer Films. *Science* **319**, 1069-1073 (2008).
- 843 40. Grossman, M. et al. Mineral Nano-Interconnectivity Stiffens and Toughens Nacre-Like
844 Composite Materials. *Adv. Mater.* **29**, 1605039 (2017).
- 845 41. Bai, H. et al. Bioinspired Hydroxyapatite/Poly(methyl methacrylate) Composite with a
846 Nacre-Mimetic Architecture by a Bidirectional Freezing Method. *Adv. Mater.* **28**, 50-
847 56 (2016).
- 848 42. Tan, G.Q. et al. Nature-Inspired Nacre-Like Composites Combining Human Tooth-
849 Matching Elasticity and Hardness with Exceptional Damage Tolerance. *Adv. Mater.*
850 **31**, 1904603 (2019).
- 851 43. Mao, L.B. et al. Synthetic Nacre by Predesigned Matrix-Directed Mineralization.
852 *Science* **354**, 107-110 (2016).
- 853 44. Tan, Y.P. et al. Infiltration of Chitin by Protein Coacervates Defines the Squid Beak
854 Mechanical Gradient. *Nat. Chem. Biol.* **11**, 488-495 (2015).
- 855 45. Gim, J. et al. Nanoscale Deformation Mechanics Reveal Resilience in Nacre of Pinna
856 Nobilis Shell. *Nat. Commun.* **10**, 4822 (2019).
- 857 46. Zeng, F.Z. et al. A Bioinspired Ultratough Multifunctional Mica-Based Nanopaper
858 with 3D Aramid Nanofiber Framework as an Electrical Insulating Material. *Acs Nano*
859 **14**, 611-619 (2020).
- 860 47. Yin, Z., Hannard, F. & Barthelat, F. Impact-Resistant Nacre-Like Transparent
861 Materials. *Science* **364**, 1260-1263 (2019).
- 862 48. Weaver, J.C. et al. The Stomatopod Dactyl Club: A Formidable Damage-Tolerant
863 Biological Hammer. *Science* **336**, 1275-1280 (2012).
- 864 49. Grunfelder, L.K. et al. Bio-inspired Impact-Resistant Composites. *Acta Biomater.*
865 **10**, 3997-4008 (2014).
- 866 50. Yang, W. et al. Protective Role of Arapaima Gigas Fish Scales: Structure and
867 Mechanical Behavior. *Acta Biomater.* **10**, 3599-3614 (2014).
- 868 51. Huang, W. et al. A Natural Impact-Resistant Bicontinuous Composite Nanoparticle
869 Coating. *Nat. Mater.* **19**, 1236-1243 (2020).
- 870 52. Yaraghi, N.A. et al. A Sinusoidally Architected Helicoidal Biocomposite. *Adv. Mater.*
871 **28**, 6835-6844 (2016).
- 872 53. Gansel, J.K. et al. Gold Helix Photonic Metamaterial as Broadband Circular Polarizer.
873 *Science* **325**, 1513-1515 (2009).
- 874 54. Urban, M.J. et al. Chiral Plasmonic Nanostructures Enabled by Bottom-Up
875 Approaches. in *Ann. Rev. Phys. Chem.*, Vol. 70 (eds. Johnson, M.A. & Martinez, T.J.)
876 275-299 (2019).
- 877 55. Ling, S.J., Kaplan, D.L. & Buehler, M.J. Nanofibrils in Nature and Materials
878 Engineering. *Nat. Rev. Mater.* **3**, 18016 (2018).
- 879 56. Nikolov, S. et al. Revealing the Design Principles of High-Performance Biological
880 Composites Using Ab initio and Multiscale Simulations: The Example of Lobster
881 Cuticle. *Adv. Mater.* **22**, 519-526 (2010).

- 882 57. Cherpak, V. et al. Robust Chiral Organization of Cellulose Nanocrystals in Capillary
883 Confinement. *Nano Lett.* **18**, 6770-6777 (2018).
- 884 58. Guo, J.Q. et al. Biodegradable Laser Arrays Self-Assembled from Plant Resources.
885 *Adv. Mater.* **32**, 2002332 (2020).
- 886 59. Lin, Y.S., Wei, C.T., Olevsky, E.A. & Meyers, M.A. Mechanical Properties and the
887 Laminate Structure of Arapaima Gigas Scales. *J. Mech. Behavior Biomed. Mater.* **4**,
888 1145-1156 (2011).
- 889 60. Yazawa, K., Malay, A.D., Masunaga, H., Norma-Rashid, Y. & Numata, K.
890 Simultaneous Effect of Strain Rate and Humidity on the Structure and Mechanical
891 Behavior of Spider Silk. *Comm. Mater.* **1**, 10 (2020).
- 892 61. Fu, C.J. et al. Cryogenic Toughness of Natural Silk and a Proposed Structure-Function
893 Relationship. *Mater. Chem. Frontiers* **3**, 2507-2513 (2019).
- 894 62. Tung, S.O., Ho, S., Yang, M., Zhang, R.L. & Kotov, N.A. A Dendrite-Suppressing
895 Composite Ion Conductor from Aramid Nanofibres. *Nat. Commun.* **6**, 6152 (2015).
- 896 63. Gupta, N., Alred, J.M., Penev, E.S. & Yakobson, B.I. Universal Strength Scaling in
897 Carbon Nanotube Bundles with Frictional Load Transfer. *ACS Nano* **15**, 1342-1350
898 (2021).
- 899 64. Guo, C.C. et al. Thermoplastic Moulding of Regenerated Silk. *Nat. Mater.* **19**, 102-108
900 (2020).
- 901 65. Jolowsky, C., Sweat, R., Park, J.G., Hao, A. & Liang, R. Microstructure Evolution and
902 Self-Assembling of CNT Networks During Mechanical Stretching and Mechanical
903 Properties of Highly Aligned CNT Composites. *Compos. Sci. Tech.* **166**, 125-130
904 (2018).
- 905 66. Pramanik, C., Gissinger, J.R., Kumar, S. & Heinz, H. Carbon Nanotube Dispersion in
906 Solvents and Polymer Solutions: Mechanisms, Assembly, and Preferences. *ACS Nano*
907 **11**, 12805-12816 (2017).
- 908 67. Davijani, A.A.B. & Kumar, S. Ordered Wrapping of Poly(methyl methacrylate) on
909 Single Wall Carbon Nanotubes. *Polymer* **70**, 278-281 (2015).
- 910 68. Eyckens, D.J. et al. Fiber with Butterfly Wings: Creating Colored Carbon Fibers with
911 Increased Strength, Adhesion, and Reversible Malleability. *ACS Appl. Mater.*
912 *Interfaces* **11**, 41617-41625 (2019).
- 913 69. Heinz, H. et al. Nanoparticle Decoration with Surfactants: Molecular Interactions,
914 Assembly, and Applications. *Surf. Sci. Rep.* **72**, 1-58 (2017).
- 915 70. Huang, Y., Sasano, T., Tsujii, Y. & Ohno, K. Well-Defined Polymer-Brush-Coated
916 Rod-Shaped Particles: Synthesis and Formation of Liquid Crystals. *Macromolecules*
917 **49**, 8430-8439 (2016).
- 918 71. Liu, Z., Xu, Z., Hu, X. & Gao, C. Lyotropic Liquid Crystal of Polyacrylonitrile-
919 Grafted Graphene Oxide and Its Assembled Continuous Strong Nacre-Mimetic Fibers.
920 *Macromolecules* **46**, 6931-6941 (2013).
- 921 72. Naguib, M. Multifunctional Pure MXene Fiber from Liquid Crystals of Only Water
922 and MXene. *ACS Central Science* **6**, 344-346 (2020).
- 923 73. Chang, H., Luo, J., Gulgunje, P.V. & Kumar, S. Structural and Functional Fibers. *Ann.*
924 *Rev. Mater. Res.* **47**, 13.1-13.29 (2017).
- 925 74. Bakhtiary Davijani, A.A., Chang, H., Liu, H.C., Luo, J. & Kumar, S. Stress Transfer in
926 Nanocomposites Enabled by Poly(methyl methacrylate) Wrapping of Carbon
927 Nanotubes. *Polymer* **130**, 191-198 (2017).

- 928 75. Asai, M., Zhao, D. & Kumar, S.K. Role of Grafting Mechanism on the Polymer
929 Coverage and Self-Assembly of Hairy Nanoparticles. *ACS Nano* **11**, 7028-7035
930 (2017).
- 931 76. Hansoge, N.K. et al. Materials by Design for Stiff and Tough Hairy Nanoparticle
932 Assemblies. *ACS Nano* **12**, 7946-7958 (2018).
- 933 77. Xu, H. et al. Obtaining High Mechanical Performance Silk Fibers by Feeding Purified
934 Carbon Nanotube/Lignosulfonate Composite to Silkworms. *RSC Adv.* **9**, 3558-3569
935 (2019).
- 936 78. Jiang, C. et al. Mechanical Properties of Robust Ultrathin Silk Fibroin Films. *Adv.*
937 *Funct. Mater.* **17**, 2229-2237 (2007).
- 938 79. Podsiadlo, P., Tang, Z., Shim, B.S. & Kotov, N.A. Counterintuitive Effect of
939 Molecular Strength and Role of Molecular Rigidity on Mechanical Properties of
940 Layer-by-Layer Assembled Nanocomposites. *Nano Lett.* **7**, 1224-1231 (2007).
- 941 80. Svagan, A.J., Samir, M.A.S.A. & Berglund, L.A. Biomimetic Foams of High
942 Mechanical Performance Based on Nanostructured Cell Walls Reinforced by Native
943 Cellulose Nanofibrils. *Adv. Mater.* **20**, 1263-1269 (2008).
- 944 81. Xiong, R. et al. Ultrarobust Transparent Cellulose Nanocrystal-Graphene Membranes
945 with High Electrical Conductivity. *Adv. Mater.* **28**, 1501-1509 (2016).
- 946 82. Munch, E. et al. Tough, Bio-Inspired Hybrid Materials. *Science* **322**, 1516-1520
947 (2008).
- 948 83. Djumas, L., Molotnikov, A., Simon, G.P. & Estrin, Y. Enhanced Mechanical
949 Performance of Bio-Inspired Hybrid Structures Utilising Topological Interlocking
950 Geometry. *Sci. Rep.* **6**, 26706 (2016).
- 951 84. Cheng, Q., Jiang, L. & Tang, Z. Bioinspired Layered Materials with Superior
952 Mechanical Performance. *Acc. Chem. Res.* **47**, 1256-1266 (2014).
- 953 85. Zhang, Y. et al. Bioinspired, Graphene-enabled Ni Composites with High Strength and
954 Toughness. *Sci. Adv.* **5**, eaav5577 (2019).
- 955 86. Raut, H.K. et al. Tough and Strong: Cross-Lamella Design Imparts Multifunctionality
956 to Biomimetic Nacre. *ACS Nano* **14**, 9771-9779 (2020).
- 957 87. Sachs, C., Fabritius, H. & Raabe, D. Influence of Microstructure on Deformation
958 Anisotropy of Mineralized Cuticle from the Lobster *Homarus Americanus*. *J. Struct.*
959 *Biol.* **161**, 120-132 (2008).
- 960 88. Gu, M., Jiang, C., Liu, D., Prempeh, N. & Smalyukh, I.I. Cellulose
961 Nanocrystal/Poly(ethylene glycol) Composite as an Iridescent Coating on Polymer
962 Substrates: Structure-Color and Interface Adhesion. *ACS Appl. Mater. Interfaces* **8**,
963 32565-32573 (2016).
- 964 89. Wang, B. & Walther, A. Self-Assembled, Iridescent, Crustacean-Mimetic
965 Nanocomposites with Tailored Periodicity and Layered Cuticular Structure. *ACS Nano*
966 **9**, 10637-10646 (2015).
- 967 90. Vollick, B., Kuo, P.Y., Therien-Aubin, H., Yan, N. & Kumacheva, E. Composite
968 Cholesteric Nanocellulose Films with Enhanced Mechanical Properties. *Chem. Mater.*
969 **29**, 789-795 (2017).
- 970 91. Chen, P.-Y., Lin, A.Y.-M., McKittrick, J. & Meyers, M.A. Structure and Mechanical
971 Properties of Crab Exoskeletons. *Acta Biomater.* **4**, 587-596 (2008).
- 972 92. Ayutsede, J. et al. Carbon Nanotube Reinforced *Bombyx mori* Silk Nanofibers by the
973 Electrospinning Process. *Biomacromolecules* **7**, 208-214 (2006).

- 974 93. Yang, J., Han, C.-R., Zhang, X.-M., Xu, F. & Sun, R.-C. Cellulose Nanocrystals
975 Mechanical Reinforcement in Composite Hydrogels with Multiple Cross-Links:
976 Correlations between Dissipation Properties and Deformation Mechanisms.
977 *Macromolecules* **47**, 4077-4086 (2014).
- 978 94. Watanabe, K. et al. Highly Transparent and Tough Filler Composite Elastomer
979 Inspired by the Cornea. *ACS Mater. Lett.* **2**, 325-330 (2020).
- 980 95. Pan, H. et al. Significantly Reinforced Composite Fibers Electrospun from Silk
981 Fibroin/Carbon Nanotube Aqueous Solutions. *Biomacromolecules* **13**, 2859-2867
982 (2012).
- 983 96. Wang, J., Cheng, Q., Lin, L. & Jiang, L. Synergistic Toughening of Bioinspired
984 Poly(vinyl alcohol)-Clay-Nanofibrillar Cellulose Artificial Nacre. *ACS Nano* **8**, 2739-
985 2745 (2014).
- 986 97. Lönnberg, H., Larsson, K., Lindström, T., Hult, A. & Malmström, E. Synthesis of
987 Polycaprolactone-Grafted Microfibrillated Cellulose for Use in Novel
988 Bionanocomposites-Influence of the Graft Length on the Mechanical Properties. *ACS*
989 *Appl. Mater. Interfaces* **3**, 1426-1433 (2011).
- 990 98. Scaffaro, R. & Maio, A. Integrated Ternary Bionanocomposites with Superior
991 Mechanical Performance via the Synergistic Role of Graphene and Plasma Treated
992 Carbon Nanotubes. *Composites, Part B* **168**, 550-559 (2019).
- 993 99. Ashby, M.F. Overview No. 80: On the Engineering Properties of Materials. *Acta*
994 *Metallurgica* **37**, 1273-1293 (1989).
- 995 100. *CES EduPack Software*, (Granta Design Limited, Cambridge, UK, 2009).
- 996 101. Dalton, A.B. et al. Super-Tough Carbon-Nanotube Fibres - These Extraordinary
997 Composite Fibres Can Be Woven into Electronic Textiles. *Nature* **423**, 703-703
998 (2003).
- 999 102. Praprotnik, M., Site, L.D. & Kremer, K. Multiscale Simulation of Soft Matter: From
1000 Scale Bridging to Adaptive Resolution. *Annu. Rev. Phys. Chem.* **59**, 545-571 (2008).
- 1001 103. Heinz, H. & Ramezani-Dakhel, H. Simulations of Inorganic-Bioorganic Interfaces to
1002 Discover New Materials: Insights, Comparisons to Experiment, Challenges, and
1003 Opportunities. *Chem. Soc. Rev.* **45**, 412-448 (2016).
- 1004 104. Lu, J.X., Luo, M. & Yakobson, B.I. Glass Composites Reinforced with Silicon-Doped
1005 Carbon Nanotubes. *Carbon* **128**, 231-236 (2018).
- 1006 105. Tsafack, T. et al. Exploring the Interface between Single-walled Carbon Nanotubes
1007 and Epoxy Resin. *Carbon* **105**, 600-606 (2016).
- 1008 106. Heinz, H., Lin, T.-J., Mishra, R.K. & Emami, F.S. Thermodynamically Consistent
1009 Force Fields for the Assembly of Inorganic, Organic, and Biological Nanostructures:
1010 The INTERFACE Force Field. *Langmuir* **29**, 1754-1765 (2013).
- 1011 107. Mason, J.A. et al. Contraction and Expansion of Stimuli-Responsive DNA Bonds in
1012 Flexible Colloidal Crystals. *J. Am. Chem. Soc.* **138**, 8722-8725 (2016).
- 1013 108. Samanta, D. et al. Multivalent Cation-Induced Actuation of DNA-Mediated Colloidal
1014 Superlattices. *J. Am. Chem. Soc.* **141**, 19973-19977 (2019).
- 1015 109. Gissinger, J.R., Pramanik, C., Newcomb, B., Kumar, S. & Heinz, H. Nanoscale
1016 Structure-Property Relationships of Polyacrylonitrile/CNT Composites as a Function
1017 of Polymer Crystallinity and CNT Diameter. *ACS Appl. Mater. Interfaces* **10**, 1017-
1018 1027 (2018).

- 1019 110. Zhao, H. et al. NanoMine Schema: An Extensible Data Representation for Polymer
1020 Nanocomposites. *APL Materials* **6**, 111108 (2018).
- 1021 111. Gooneie, A., Schuschnigg, S. & Holzer, C. A Review of Multiscale Computational
1022 Methods in Polymeric Materials. *Polymers* **9**, 16 (2017).
- 1023 112. Ha, Y. & Bobaru, F. Studies of Dynamic Crack Propagation and Crack Branching with
1024 Peridynamics. *Int. J. Fracture* **162**, 229-244 (2010).
- 1025 113. Vassaux, M., Sinclair, R.C., Richardson, R.A., Suter, J.L. & Coveney, P.V. The Role
1026 of Graphene in Enhancing the Material Properties of Thermosetting Polymers. *Adv.*
1027 *Theory Simul.* **2**, 1800168 (2019).
- 1028 114. Guarin-Zapata, N., Gomez, J., Kisailus, D. & Zavattieri, P.D. Bandgap Tuning in
1029 Bioinspired Helicoidal Composites. *J. Mech. Phys. Solids* **131**, 344-357 (2019).
- 1030 115. Gu, G.X., Chen, C.T., Richmond, D.J. & Buehler, M.J. Bioinspired Hierarchical
1031 Composite Design Using Machine Learning: Simulation, Additive Manufacturing, and
1032 Experiment. *Materials Horizons* **5**, 939-945 (2018).
- 1033 116. Kronqvist, N. et al. Efficient Protein Production Inspired by How Spiders Make Silk.
1034 *Nat. Commun.* **8**, 15504 (2017).
- 1035 117. Valois, E., Mirshafian, R. & Waite, J.H. Phase-Dependent Redox Insulation in Mussel
1036 Adhesion. *Sci. Adv.* **6**, eaaz6486 (2020).
- 1037 118. Wang, C.Y., Xia, K.L., Zhang, Y.Y. & Kaplan, D.L. Silk-Based Advanced Materials
1038 for Soft Electronics. *Acc. Chem. Res.* **52**, 2916-2927 (2019).
- 1039 119. Wu, Z. et al. A Comprehensive Survey on Graph Neural Networks. *IEEE Transactions*
1040 *on Neural Networks and Learning Systems* **32**, 4-24 (2021).
- 1041 120. Wang, M.Q. et al. Biomorphic Structural Batteries for Robotics. *Science Robotics* **5**,
1042 eaba1912 (2020).
- 1043 121. Yu, C.H., Qin, Z., Martin-Martinez, F.J. & Buehler, M.J. A Self-Consistent
1044 Sonification Method to Translate Amino Acid Sequences into Musical Compositions
1045 and Application in Protein Design Using Artificial Intelligence. *ACS Nano* **13**, 7471-
1046 7482 (2019).
- 1047 122. Jin, W., Barzilay, R. & Jaakkola, T. Hierarchical Generation of Molecular Graphs
1048 using Structural Motifs. in *Proceedings of the 37th International Conference on*
1049 *Machine Learning* Vol. 119 (eds Hal, D., III & Aarti, S.) 4839-4848 (PMLR,
1050 Proceedings of Machine Learning Research, 2020).
- 1051 123. Lossada, F., Jiao, D., Hoenders, D. & Walther, A. Recyclable and Light-Adaptive
1052 Vitrimer-Based Nacre-Mimetic Nanocomposites. *ACS Nano* **15**, 5043-5055 (2021).
- 1053 124. Xin, A. et al. Growing Living Composites with Ordered Microstructures and
1054 Exceptional Mechanical Properties. *Adv. Mater.* **33**, 2006946 (2021).
- 1055 125. *CRC Handbook of Chemistry and Physics*, (CRC Press, Boca Raton, FL, 2020).
- 1056